1969

A study of bias susceptibility characteristics of thin permalloy films

Chester St John Comstock Jr.
Iowa State University

A STUDY OF BIAS SUSCEPTIBILITY CHARACTERISTICS OF THIN PERMALLOY FILMS

by

Chester St. John Comstock, Jr.

A Dissertation Submitted to the
Graduate Faculty in Partial Fulfillment of
The Requirements for the Degree of
DOCTOR OF PHILOSOPHY

Major Subject: Electrical Engineering

Approved:

Signature was redacted for privacy.

In Charge of Major Work

Signature was redacted for privacy.

Head of Major Department

Signature was redacted for privacy.

Dean of Graduate College

Iowa State University
Ames, Iowa

1969

TABLE OF CONTENTS

I. INTRODUCTION

A. Background and Review

Considerable effort has been expended in the past decade in an attempt to obtain an adequate model and a corresponding mathematical description of the structure and behavior of a thin ferromagnetic film. This thesis is primarily concerned with the physical model aspect of the problem and it is based upon the support and extension of existing theories pertaining to a description of the local magnetic behavior of a thin ferromagnetic film as a function of applied fields. This description, in turn, is based upon experimental techniques and the resulting bias susceptibility measurements. This first section consists of a brief review of some of the more significant observations and theories to date.

It was convenient for early investigators to assume that a magnetic film behaved as an ideal single domain structure (1) and that the magnetic material possessed a completely homogeneous uniaxial anisotropy throughout the film volume. This assumption was justified in that it certainly facilitated the understanding of many of the observed phenomena. However, it was soon found that typical permalloy films were far from ideal in this respect, and that explanations of some of the observations could not ignore the fact that inhomogenities were present. These inhomogenities manifest themselves as locally varying forces which acted on the magnetization, the effect of which was observed experimentally (2, 3, 4). These observations were believed to be due to a variation of the uniaxial anisotropy in direction and magnitude from point to point throughout the volume of the film. These effects were known as angular and magnitude anisotropy

dispersion respectively (5, 6).

An explanation of these observations might be effected by assuming that the film was composed of many small non-interacting regions (2) each of which acts as an ideal uniaxial domain (1) with its own easy axis orientation and magnitude of H_k which are distributed in an approximate Gaussian manner about the average easy axis and average H_k of the film (5). Two of the more widely used experimental techniques which were proposed to measure this dispersion characteristic from the film as a whole, were presented by Crowther (2) and Torok (5). The first method, by Crowther (2, 6), involves measuring the distribution of easy axes (angular dispersion) by saturating the film in approximately the hard direction, and, upon relaxing the field to zero, by noting the percentage of the film in which the magnetization rotates towards the original easy direction as opposed to the opposite easy direction. The second technique, which also derives its measurements from the entire film, was proposed by Torok (5) and measures quantities related to both the orientational and magnitude dispersions. It does this by measuring the imaginary (loss) part of the complex bias susceptibility. This quantity is the magnetic flux varying in time quadrature with a small ac tickle field. In the measurements a dc bias field is also applied simultaneously with and perpendicular to the small tickle field. The measurements were involved, in field space, near the hard axis tip of the Stoner-Wohlfarth rotational switching threshold curve (1). It was assumed (5) that the observed loss represented the irreversible switching of many of the small domain type regions in the film. In other words if the hard axis tip of the switching asteroid

describing a small region in the film was located such that the small ac tickle field crossed it, it would switch irreversibly and contribute to loss. There are other experimental techniques available to measure the inhomogeneity in the anisotropy a list of which appears in References 7-9.

Other models have been proposed in an effort to explain the observed small-amplitude loss phenomenon and its dependence on a dc bias field. Smith (10) considered the film to be composed of small regions possessing negative anisotropy, where the local easy axis was perpendicular to the average easy axis of the film. This was thought to be the case when loss was observed, in films of $H_c/H_k > 1$, near the 180^o threshold of the switching asteroid. This model was later confirmed by Doyle et al. (11) who used it to explain the observed hysteresis in torque measurements and the relationship with coercive force.

Another theory was advanced by Torok (12) in an effort to explain the negative anisotropy and other observations. He proposed a model of the magnetic structure which was based on the existence of small regions in the film which possessed an effective combination of uniaxial and biaxial anisotropies. He called it complex biaxial anisotropy. The biaxial contribution is random in nature throughout the film.

Coren and Juretschke (13) suggested the film structure was composed of an array of randomly oriented non-interacting equivolume elements with uniaxial anisotropy superimposed on an overall uniaxial anisotropy. Cundall and King (14) published an independent comparison between the theories of Torok (12), Coren and Juretschke (13) and a yet to be discussed ripple theory. They showed that there was good agreement between these first two theories and experiment. The quantity they compared was α_{90} (2, 5)

as a function of film composition.

In a later paper on this same subject Torok (7) furthered the theoretical considerations pertaining to his complex biaxial anisotropy model. In this paper he reviewed and compared some existing theories and discussed in some depth the micromagnetic factors influencing the formation of ripple. He also obtained an expression for the ripple wavelength at $H_{90} \simeq H_k$ by bringing in nonlinear field terms. A review and discussion of Torok's (7) work was presented by Uchiyama et al. (15) in relation to their own work on the origin of the random anisotropy in magnetic films.

One objection to all these models, with the exception of the last one of Torok's (7), is the assumption that the small domain sized regions are basically non-coupled. This is not physically realizable. Another common tie between these models was the expressed or implied interpretation that the observed loss represented the irreversible switching of the independent randomly distributed regions of either uniaxial, negative, or complex biaxial anisotropy. These observations took place near the hard axis tip or near the 180° easy axis tip of the switching asteroid with apparently negligible loss in between.

Most of the other theoretical contributions, whether mathematical or qualitative in nature had as a basis the so called ripple theory. This theory was initiated by the independent experiments of Fuller and Hale (16, 17) and Boersch and Raith (18). They demonstrated a technique of defocusing a transmission electron microscope such that the fine structure of the magnetization configuration in a thin polycrystalline film could be observed. This technique, known as Lorentz Microscopy, is based on the

fact that electrons, on passing through a magnetic film, experience a deflection caused by interaction with the magnetization of the sample, i.e. the Lorentz force. The resolution of the observations is of the order of a fraction of a micron.

The results of these experiments showed not only the existence of domains and domain walls, as expected, but also a magnetic fine structure within each domain. This fine structure consisted of small variations in the direction of the magnetization. They were observed as long approximately parallel strips of uniform intensity, situated transverse (perpendicular) to the direction of the mean magnetization. The magnetization was parallel within each strip but varied in direction from strip to strip. These small roughly periodic magnetic striations are known as the magnetization ripple (17).

Since its inception this wavelike ripple structure has been observed through the use of Lorentz Microscopy by many experimenters. One of the most noteworthy is Cohen (19, 20). Its inception also stimulated a number of theoretical treatises in an effort to mathematically explain the phenomenon (7, 8, 21-28). This stimulation came about because it was recognized by most of these authors that this picture of the magnetic structure represented an optimum model. It represented the bridge between the now known fact that inhomogeneities in the magnetic material causing nonuniformities in the magnetization direction did exist and some picture or model of what they looked like. The early theories of small domain sized areas now could be tied in directly with the ripple structure.

These theoretical works in turn stimulated a considerable amount of

experimental work in an attempt to prove the theories correct, or incorrect as the case might be. Another incentive, more fundamental than the first, came from the fact that the actual underlying physical causes of the magnetization ripple were (and still are) not completely understood. It is now accepted that the wall free ripple structure is the result of the interaction of various forces on the local magnetization, i.e. exchange, magnetostatic (demagnetizing or stray), applied field, and two of magnetic anisotropy origin (7, 8, 22, 26, 29). It is these last two that aren't completely understood. One is the uniaxial anisotropy force induced during fabrication and is considered to be more or less constant throughout the film. The other is believed to be random in nature, varying locally in direction and magnitude from crystallite to crystallite in the polycrystalline film. The origin of the former has been the subject of researchers for some time. The origin of the local anisotropy force is thought to be magnetocrystalline (17, 30, 31) or stress-magnetostriction (6) or a combination of both (7, 8, 15, 22, 32) in nature. An excellent review article discussing and listing many of the experimental publications is Reference 8 by Harte.

The theoretical offerings referenced above are all based upon the fact that the ripple structure is constructed as Fuller and Hale (17) originally described it, which is that the wave fronts of the ripple striations represent the fluctuation of the magnetization direction about a mean direction, and that the mean direction is perpendicular to these wave fronts, i.e. longitudinal ripple. This conclusion is obtained by stray field considerations and is done in an elegant manner by Harte (8).

A brief description of the method of attack used by a few of these

authors might be in order. Hoffmann (22, 23) started his developments from an energy standpoint. This facilitated taking derivatives with respect to a local angle variable from which equilibrium and instability may be derived. He then used variational techniques to obtain a differential equation, from which he extracted a term to effect a linear equation which greatly facilitated solving. The nonlinear term he eliminated was one proportional to the longitudinal (parallel to the mean direction of $\vec{M}$) stray field. The quantities he solved for were the rms value of the ripple angle, the ripple wavelength, the incremental susceptibility, and the mean value of the demagnetizing field. His nonlinear theory is not yet complete, although the linear theory is. A review and comparison of some of Hoffmann's results are in a paper by Leaver et al. (33).

The theory of Harte (8), which to the knowledge of this author is the most complete treatment yet published, has obtained a solution including the effects of the nonlinear terms. He started with the same basic terms as Hoffmann except in local torque equilibrium form. All torque contributions were expanded into a sum of Fourier components. The sum of the components for a given wave number were then equated to zero which gave rise to an expression for the Fourier component of the ripple angle. This angle was found to be equal to the corresponding Fourier component of the local anisotropy field divided by an effective field. The effective field included nonlinear terms from longitudinal magnetostatic and uniform fields. These fields came in through third order torque contributions. After a rather complicated averaging process of a very complicated expression for the effective field, an expression for the rms ripple

amplitude was found in terms of characteristic coherence lengths, which also determined the dimensions of the "ripple domain". The ripple expression was found as a limiting case of these lengths which in turn were defined by the scale of the inhomogeneity and the film thickness. The final expression for the rms ripple amplitude was twofold to account for the transition from the quasilinear to nonlinear theory as the ripple amplitude increased.

Callen et al. (26) and Feldtkeller (28) offered theories more phenomenological in nature than those of Hoffmann and Harte. Callen, using the theory of the apparent periodicity of random numbers, derived an expression for the rms value of the local transverse component of the magnetization. His results agreed quite closely with measurements taken from ripple structure pictures and with the theoretical results of Rother (21), and the experimental results of Baltz and Doyle (34).

Feldtkeller's ripple field theory (28) was initiated by assuming the existence of relatively large longitudinal stray fields. They were then expressed in terms of an average ripple field acting parallel to the mean magnetization. He then solved for the transverse susceptibility. A review and comparison of his work with others appears in Reference 33 by Leaver et al.

Feldtkeller (27) was also the originator of a model explaining the loss phenomenon observed by the quadrature flux technique (5). This model is quite consistent with the basic ripple theory in that it was originally observed through Lorentz microscope pictures. Feldtkeller postulated that the observed loss was due to the irreversible rearrangements of the magnetization ripple taking place under the influence of the

applied tickle field. The loss became known as ripple hysteresis. A very good review and experimental treatment, through susceptibility measurements, of this theory is given by Harte et al. (35).

B. Purpose

It is known (5, 33, 36) that complex bias susceptibility measurements are sensitive to variations in the magnetic structure of a ferromagnetic thin film. This thesis will be concerned with the use of susceptibility measurements as a means through which the local magnetic properties of a film can be related to the macroscopic magnetic observations.

In this investigation a technique, heretofore unreported, will be presented for the determination of the average rms ripple angle for a particular region of field space. The same basic technique will also be used to obtain a quantitative measure of some of the internal fields which are present when the film sample is in a splitting domain configuration. These processes use the curves which result from measurements of the real part of the bias susceptibility, X'_{jj}, and the integral of the X'_{jj} vs H_j curves.

It will be useful and most convenient to make reference throughout the discussions in this thesis to the rotational switching threshold asteroid for ideal single domain particles as developed by Stoner and Wohlfarth (1). It is realized that this curve, in part, represents a nonrealistic ideal case, but nonetheless it is a very handy reference. Field points and trajectories can be drawn and located and talked about with regard to their proximity to each other and the threshold asteroid.

Many susceptibility measurements have been taken as the bias field is

decreased from large saturation values back to zero. However, much interesting information can also be obtained by examination of the characteristic which results from setting the film initially in a single domain state and increasing the bias field from zero to saturation values. An interpretation of the loss mechanism and ripple behavior will be given for the magnetic configuration which is a result of both increasing and decreasing bias field conditions. The discussion will show that one of the most important factors governing thin film behavior, and the resulting measured curves, is internal magnetostatic (stray) fields. These fields come from the divergence of the magnetization within the ripple structure itself. This field can be accompanied by a pinning or locking of the ripple or wall structure. This effect is very important in explaining the shape of and differences between susceptibility curves. The observation that the peaks of the $X_{0,90}$ curves occur at values of $H_{90} > H_k$ is explained by ripple pinning and associated demagnetizing fields.

Although not all the causes are known, the ripple structure itself, as seen by the Lorentz microscope pictures of Cohen (19, 20), the microphotometer traces of Baltz (30), and described by Hoffmann (22, 23) and Harte (8), can be thought of as sinusoidal fluctuations of the magnetization which are dependent upon the applied fields and the material. Superimposed upon this fundamental wave structure are higher frequency components which are believed to be directly a function of the crystallite size of the polycrystalline material. The larger the "dispersion", which will be taken to be an intrinsic measure of the larger grain size, the larger is the measured α_{90} and resulting ripple wavelength and amplitude.

A technique will be discussed whereby from measurements of X'_{jj}, where $j = 0^o$, 45^o, 90^o, it is possible to come up with values of the rms ripple angle, $\bar{\varphi}_j$, for a region of field space. The relative congruence of the resulting curves of $\bar{\varphi}_j$ vs H demonstrate that the ripple structures are quite similar for equal field magnitudes H, where H is measured along a path tangential to the asteroid and is zero at the point of tangency. The curves should be in closer theoretical agreement for values of H greater than approximately $2H_k$. This is due to the small ripple angle, negligible nonlinear effects and symmetric force distribution about the axis of the mean magnetization. This same effect was demonstrated by Harte et al. (35) using loss characteristics, X''_{jm}. A picture showing the relation between the asteroid, field path, and simplified ripple structure is shown in Figure 1a.

This same method also leads to an evaluation of the average angle the magnetization in a given domain makes with the EA when the film is in a splitting domain configuration. It also leads to the angle the mean $\vec{M}$ makes with the ED when the film is in a single domain configuration. All of these angles are functions of the applied bias field. The splitting (strip) domains referred to above compose the finely spaced domain structure, commonly observed by Bitter and other techniques, which results from saturating the film along the average HA and then decreasing the field to less than H_k. These domains are about 30-50:1 length to width, are about 5-50μ in width, and are on the average parallel to the EA.

If the film is in a strip domain configuration, by using the angle described above and the measured values of $X'_{0,90}$ and $X'_{90,90}$, it is possible to solve for some of the internal stray fields which come about as a result

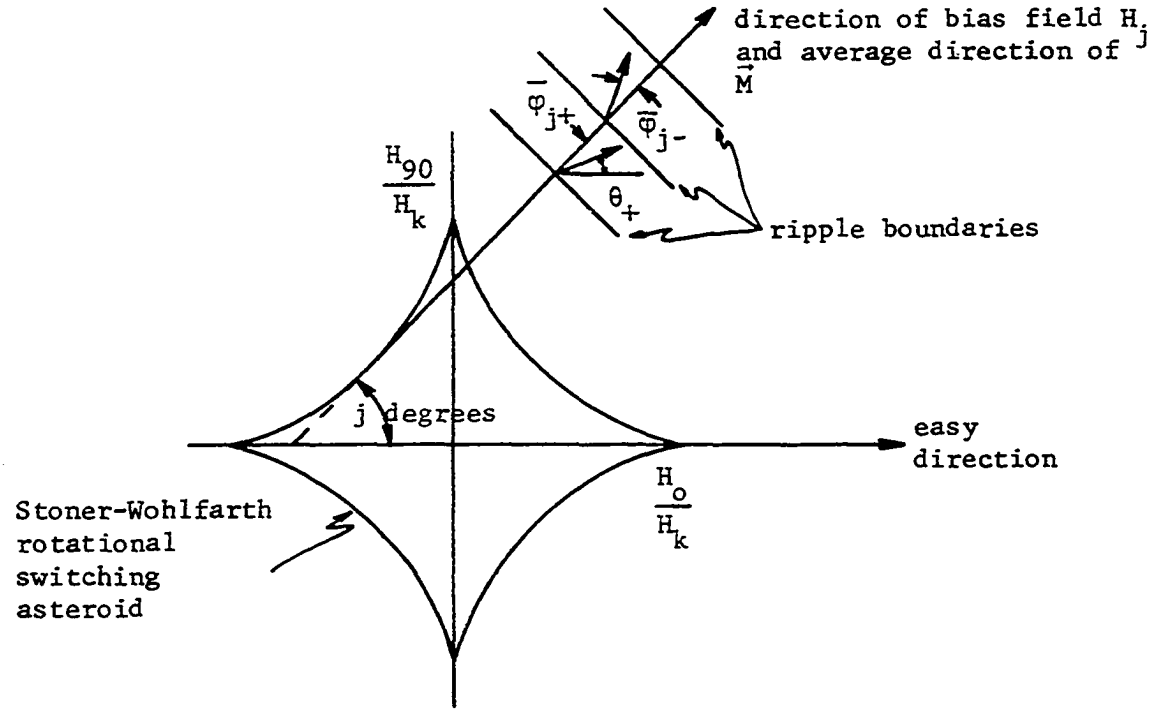

Figure 1a. Simplified picture showing relation between the asteroid, ripple structure, rms ripple angles, $\bar{\varphi}_j$, and field path H_j

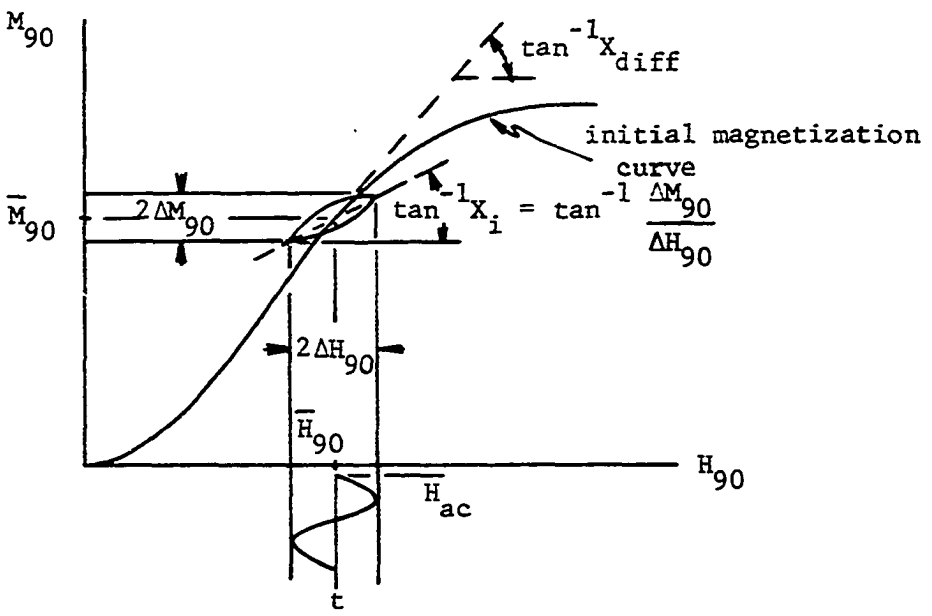

Figure 1b. Illustration of incremental and differential susceptibilities

of the tickle field applied parallel to both the EA and HA as a function of H_{90}. The technique used to do this was a torque balance before and after the application of a tickle field in both directions. This showed that the demagnetizing field contribution, which is induced by the application of an EA tickle field, is very large and is primarily responsible for the differences in the increasing and decreasing curves of $X_{0,90}$.

Comparisons were made between the experimental results of this thesis and some of the theoretical results of Hoffmann (23). The quantities compared were the rms ripple amplitude, X_{jj} versus applied field, and a calculation of the blocking field which is approximately at the peak of $X'_{0,90}$. The agreement was close except for the blocking field.

Two relatively recent reports (15, 37) on the problem of skew in thin films were considered. This very large wavelength inhomogeneity can completely mask the X'_{jj} measurements believed to be due to ripple. However, the low H_c/H_k film used in this thesis, sample 5Ba, was cut from the center of a large 3 in x 1½ in film. This coupled with the fact that near ideal alignment in the measuring apparatus was achieved led to the conclusion that the skew component was very very small. An after-the-fact indication of negligible skew was the fairly close agreement between this and Hoffmann's and Leaver's mathematical predictions.

Two other films were examined which were rectangular in shape. They had a length to width ratio of about 10 to 1 with the long dimension approximately 13mm. The EA was parallel to the long dimension in one and perpendicular to it in the other. These films were also cut from the center section of the same large film as sample 5Ba. The measurements on these

films showed the effect of shape anisotropy or edge demagnetizing fields.

C. Discussion of Susceptibility

As seen in some textbooks (38, 39) on magnetism the term magnetic susceptibility, X, can have a number of interpretations in reference to a ferromagnetic material. Some of these include initial, normal, incremental, and differential susceptibilities. All terms of this nature make reference to the macroscopic M-H hysteresis characteristic typical of these materials. The first two refer respectively to the slope of the initial M-H curve at H=0, and the slope of a line from the origin to any point on the normal magnetization curve. The last two are of primary importance as far as this thesis is concerned. The incremental susceptibility, X_i, is usually defined (38, 39) as the slope of the straight line connecting the tips of a minor hysteresis loop centered on the field axis about an arbitrary dc bias field. The loop is usually observed as the result of a small sinusoidally varying "tickle" field whose average value coincides with the dc field. This small field causes the average magnetization to rotate a small amount, ΔM, about its equilibrium value, $\bar{M}$, dictated by the peak value, ΔH, of the tickle field. This is illustrated in Figure 1b for an initial macroscopic hard-direction (90^o) M-H curve. The differential susceptibility, X_{diff}, is just the slope of the macroscopic curve at a given field value.

For present purposes the above definition of the incremental susceptibility is not complete, so another concept must be introduced to account for the fact that the small loop encompasses a finite area. This comes about because of the fact that walls or ripple boundaries are

irreversibly moved under the influence of the small time-varying field, and energy is expended in the process. This energy comes from the applied field and is proportional to the area enclosed by the loop. It can be shown (40) that this energy dissipation or loss can be formally accounted for by allowing the susceptibility to be complex. This is commonly written as $X_i = X_i' - jX_i''$, where the real part is proportional to an equivalent inductance and the imaginary part to an equivalent resistance (or energy stored and energy dissipated). This can also be seen by considering a typical situation in which the small applied ac field is in for instance the x-direction, and its time varying form is $H_x = |\Delta H_x| e^{j\omega t}$. The corresponding component of induced magnetization in the x-direction could then be written as $M_x = |\Delta M_x| e^{j(\omega t - \delta)}$. It is seen that a component of M_x exists in time quadrature with H_x. δ is called the loss angle, and the complex incremental susceptibility could be expressed as

$$X_i = \frac{M_x}{H_x} = \left|\frac{\Delta M_x}{\Delta H_x}\right| (\cos\delta - j\sin\delta)$$

If the magnitude of the small ac tickle field were reduced it would be logical to assume that in the limit as this field approached zero, $X_i \rightarrow X_{diff}$. If the ac field were small, a very good approximation would be that $X_{diff} \simeq |X_i' - jX_i''|$, where all the X's are functions of a dc bias field, and for most situations $X_i'' \ll X_i'$. It was experimentally demonstrated for regions in field space where X_i'' was negligible, that X_i' as a function of the magnitude of the tickle field was very close to being constant in value as the tickle field approached zero through the values used in the experiment. This was also observed by Feldtkeller (28).

Therefore a good approximation is $X_{diff} \simeq X_i'$ for regions of low loss. This approximation also excludes irreversible changes in the magnetization (partial rotation or wall switching) which take place as a function of the bias field and are not observed through the applied tickle field mechanism.

In texts on magnetic resonance (40), the incremental susceptibility is related in more general terms to the small applied ac tickle field, $\vec{\Delta H}$, and the induced magnetization, $\vec{\Delta M}$, as

$$\vec{\Delta M} = \overleftrightarrow{X}(\vec{\Delta H})$$

where $\overleftrightarrow{X}$ is a complex tensor, and the Δ's are used to denote incremental quantities, as before. This is more conveniently written in terms of matrix elements, as

$$\Delta M_j = X_{jm}(\Delta H)_m$$

where one possible expansion could be

$$X_{xy} = \left(\frac{\Delta M_x}{\Delta H_y}\right)_{\substack{\Delta H_x = 0 \\ \Delta H_z = 0}}$$

It will be assumed that the only X of interest is X_{jj}, where the components of ΔM and ΔH are parallel, and that ΔH_j is the only applied tickle field (all others are zero). This being the case it would be convenient, as far as the present problem is concerned, to deviate from the above established subscript nomenclature. Since all the susceptibilities are functions of a dc bias field, which will either be parallel, antiparallel, or perpendicular to the j axis, the subscripts of X_{jm} will now mean

$$X_{jm} = \left(\frac{\Delta M_j}{\Delta H_j}\right) H_m$$

where j = axis parallel to ΔM and ΔH (bi-directional)

m = axis parallel to dc bias field (uni-directional)

The designation will be in degrees counterclockwise from the average easy direction (ED) of the film, i.e. $X_{45,135}$ means ΔM and ΔH at 45° and H_{bias} at 135° to the ED (or $X_{45,135} = \left(\frac{\Delta M_{45}}{\Delta H_{45}}\right) H_{135}$).

II. EXPERIMENTAL EQUIPMENT AND TECHNIQUES

In general the experimental equipment consisted of a modified Torok (5) type bias susceptibility apparatus. More specifically the film sample lay on a rotatable platform at the center of four sets of fixed Helmholtz field coils (38). The plane of the platform, and the film, was such that it was always parallel to the fields from the four sets of coils. This arrangement is seen in Figure 2 together with some of the associated circuit components. The rotational feature allowed any angular orientation of the film with respect to the applied fields to be achieved. This could be done with an accuracy of about $\pm 0.2^{\circ}$. Two sets of these mutually orthogonal coils were used to apply any or both of two dc bias fields as well as the simultaneous application of a very small ac tickle field. The dc fields were adjustable from zero to about 15oe depending upon which coils and which sources were used. The tickle field had a usable range from about 5 to 75 moe peak value. Two 1h chokes and capacitive series tuning provided isolation between the dc supply and the ac source which was a crystal controlled oscillator of about 5kc. The other two sets of perpendicular field coils were used to cancel stray dc fields (earth).

As seen in Figure 2 the sensing arrangement consisted of a figure-8 pickup coil modified in the form of two back to back Ds. It is situated immediately under the film platform and can also be rotated such that either of two orthogonal orientations can be used. In series with the pickup coil was an adjustable bucking coil which was used to cancel any component of the applied tickle field which might be sensed by the pickup

Figure 2. Diagram showing two sets of drive field coils, the pickup coil, and part of the drive circuit

Drive Arrangement

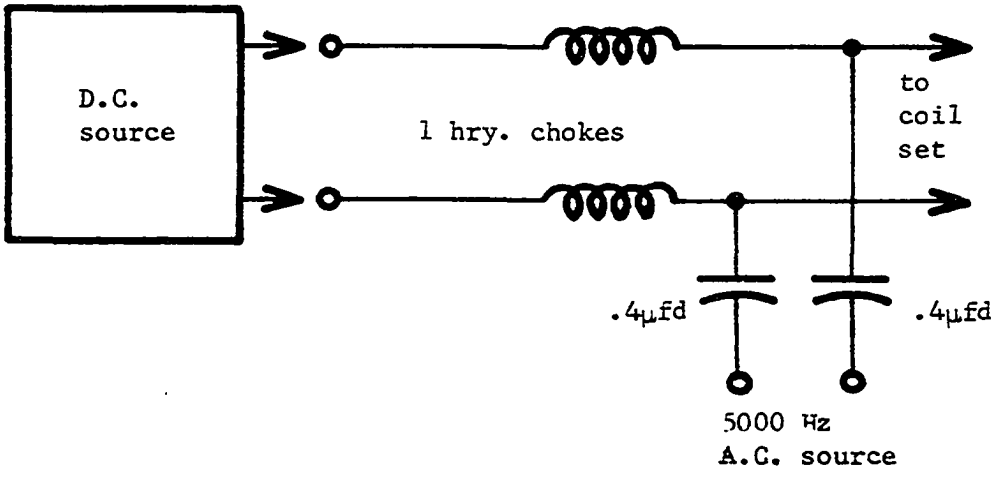

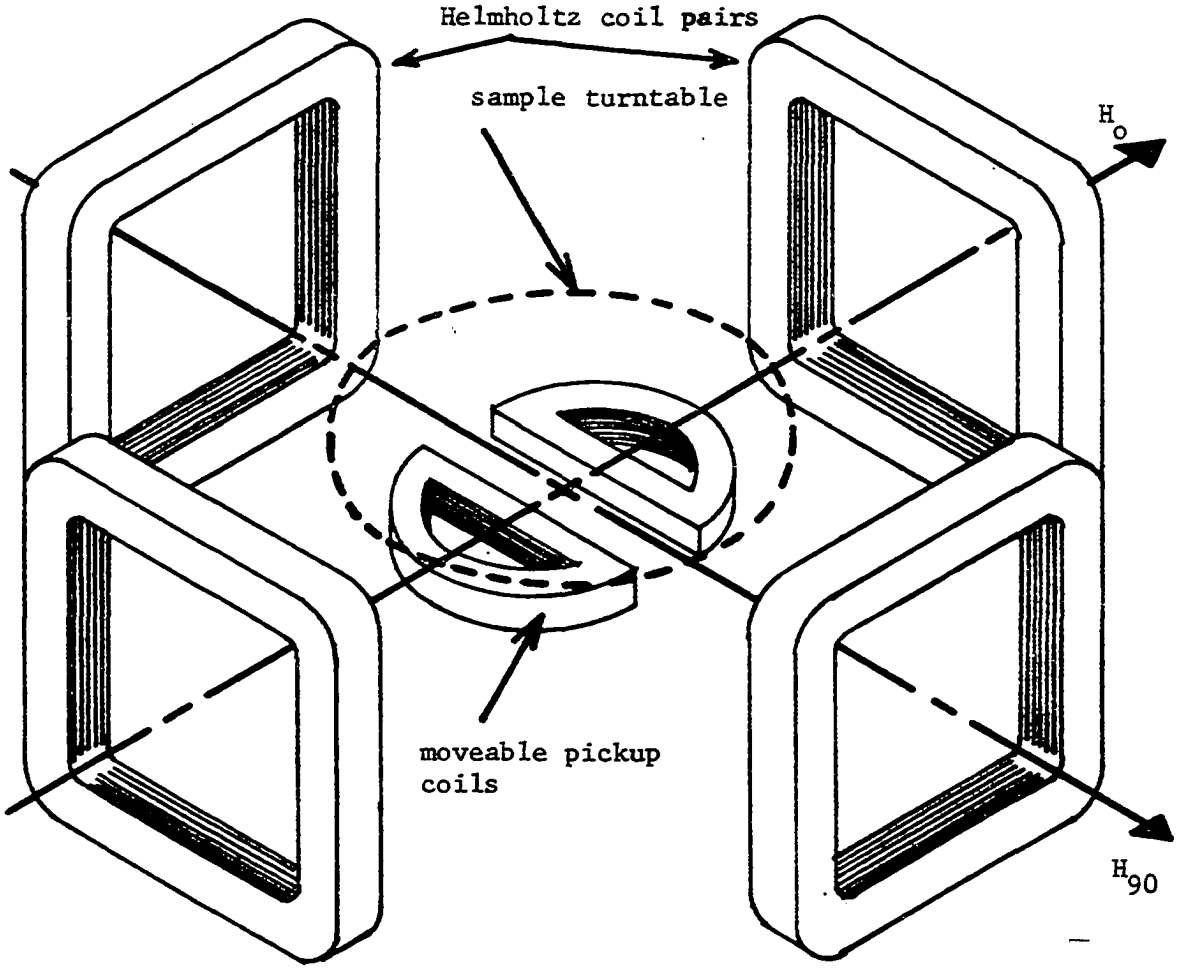

coil due to mechanical unbalance or stray pickup. This coil was also used to inject an in-phase signal for calibration purposes.

The signal induced in the pickup coil by the film was fed to a stable, highly tuned, high gain, amplifier. The reason for this was that the signal of interest was in effect the sum of two very low magnitude signals, separated by 90°, at the fundamental frequency (5kc). These two signals comprise the in and quadrature phase (real and imaginary) components of ΔM_j with respect to the applied tickle field, ΔH_j. It was desired to separate these two signals where the quadrature component was of extremely low level. This necessitated high stability, gain, and tuning, and a minimum of noise in the amplifying system.

To effect a meaningful output with the proper phase relationship between the two component signal and the applied tickle field, the signal was fed into a sampling circuit. The result of this circuit was the generation of two sets of sampling pulses, 90° apart, which were derived from the tickle field. These pulses were positioned timewise so that they occurred simultaneously with the positive peaks of the in and out of phase components of the signal. The signal was used to modulate these phase locked pulses the result of which was peak-amplitude detected and fed to the vertical input of an x-y recorder. This means that the y-input signal could be considered a time stationary quantity in that it was proportional to the magnitude of ΔM_j which in turn was solely a function of the value of the dc bias field. Calibration was effected by adjusting the phase of the composite pulse train in relation to a signal void of a loss component so the quadrature output was zero.

To complete the equipment needed to effectively automate the plotting of a susceptibility curve a varying dc bias field was needed. This was accomplished by using an RC charging, and discharging, characteristic with a conveniently long time constant. The output of this device was fed to the appropriate drive field coil and to the horizontal input of the x-y recorder.

It might be prudent to mention at this point that although the actual quantity being measured is proportional to the magnitude of ΔM_j; since the corresponding tickle field ΔH_j is always constant for a given curve, the ordinate (dependent) variable will be $X_{jm}(= \frac{\Delta M_j}{\Delta H_j})$ on all curves.

Most of the susceptibility measurements were made using a tickle field of 20moe peak value. The only exception to this was an increase to 75moe for the $X'_{0,180}$ measurements where the signal output was just too low at 20moe.

The values of H_k for the film samples were obtained by three separate techniques. One was by the usual oscilloscope projection of the initial hard direction susceptibility curve to its intersection with M and the corresponding field value. This technique is not very accurate if substantial ripple pinning occurs, although an ED bias field can correct for this. Another method was a modified torque magnetometer process which involves physically rotating the single domain film and then forcing the average $\vec{M}$ back into alignment with the original ED and noting the field required to do so. The third technique involves extrapolation of $(X_{jm})^{-1}$, where j,m = 90,0 and 0,90, back to intersect the dc field axis. The intersections are at $\pm H_k$ and their difference is $2H_k$ (28).

Four film samples are considered in this thesis. Two are round, approximately 8mm in diameter and 1000Å thick. The other two are rectangular and approximately 1.3mm x 13mm. The latter two are different in that the ED is parallel to the long dimension on one and the short dimension on the other. The round samples differed primarily in their dispersion characteristics, having an α_{90} of approximately 3.5° and 1° for samples II and 5Ba respectively. These round samples had no macroscopically observable biaxial or negative anisotropy contributions as experimentally observed by a modified torque magnetometer.

All samples were cut from the center section of large 1½in x 3in, 1000Å thick, film sheets. This was necessary to eliminate as best as possible any effects due to large scale non-uniformities or skew. If present, skew can give rise to very misleading results in measurements of X_{jj}. Sample 5Ba and the two rectangular ones were all cut from the center section of the same film sheet.

To align the film as accurately as possible in the apparatus, so the average EA was within a small fraction of a degree of being parallel to the applied EA bias field and to effectively cancel all stray (earth) fields, the increasing characteristic (from single domain state) of $X'_{0,90}$ was used, as seen in Figure 3. This provided a very sensitive test to ensure that the above criteria were met. Four curves were plotted on top of one another, one for each initial setting of the ED and one for each direction of H_{90}.

These same $X'_{0,90}$ measurements, and the resulting four curves, were also used as a means of checking on the presence of skew. To demonstrate

this two round samples were cut from the same large film as 5Ba. One came from an edge near the center of the long dimension which was parallel to the ED, and the other came from a corner. It was impossible to get all four curves to coincide by either varying the azimuth of the drive field or changing the magnitude of the stray field contribution or both. Quite close agreement was observed in pairs. The members of one pair came from opposite initial easy directions and opposing HA drives. These results were interpreted as showing the presence of skew which apparently contained an asymmetric component.

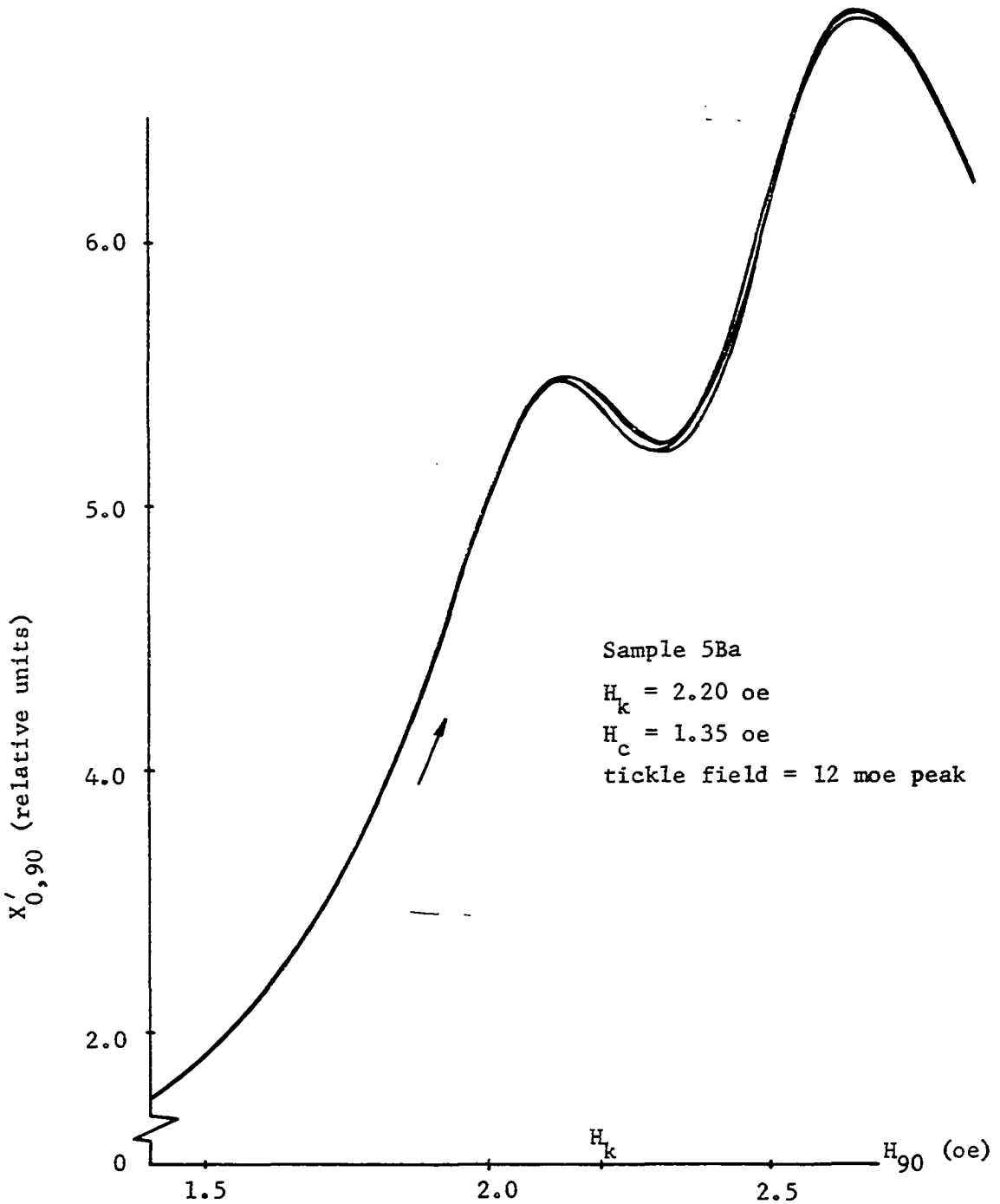

Figure 3. $X'_{0,90}$ versus H_{90} for sample 5Ba showing the four curves which result by applying H_{90} along $\pm 90^{o}$ for both initial settings of the easy direction. Only a portion of the increasing characteristics are shown

III. THEORY

A. Evaluation of RMS Ripple Angle

From the discussion of susceptibility in the introduction, the following definitions were made:

$$X_{jm} = \left(\frac{\Delta M_j}{\Delta H_j}\right)_{H_m} = X'_{jm} - jX''_{jm}, \tag{1}$$

and for situations where $X'' \ll X'$,

$$X_{jm} \simeq X'_{jm} \simeq \left(\frac{dM_j}{dH_j}\right)_{H_m}. \tag{2}$$

This section of the thesis will be concerned with an experimental-numerical technique for finding the rms ripple angle for a region of field space. In this process the tickle and bias fields are parallel, so the subscripts j and m are equal and will assume the values 0°, 45°, and 90°.

If the above expression for X'_{jj} is integrated, from $M_j(H_j)$ to $M(H_j=\infty)$,

$$\int_{M_j}^{M} dM_j = \int_{H_j}^{\infty} X'_{jj}\, dH_j \tag{3}$$

M is the saturation magnetization and is assumed constant over the film volume. Expanding, dividing by M and rearranging,

$$\frac{\bar{M}_j}{M}(H_j) = \overline{\cos\varphi_j(H_j)} = 1 - \frac{1}{M}\int_{H_j}^{\infty} \overline{X'_{jj}}\, dH_j \tag{4}$$

where the notation (H_j) is to emphasize the fact that M_j and $\cos\varphi_j$ are functions of H_j. The bar $(\bar{\ })$ denotes a volume average value. The averaging is necessary since these quantities are defined at a specific point in space but in the present context are the result of macroscopic

measurements taken over the entire volume of the thin film. So these variables, as will all which are the direct or indirect result of measurement, have to be averaged over the volume of the film sample.

A general physical interpretation of the preceding equations begins with the fact that the susceptibility, X_{jj}, or for negligible loss the slope of the macroscopic $M_j - H_j$ curve, is measured parallel to the j axis along which the dc field, H_j, is applied. The bias field is applied in two ways resulting in two distinct characteristics. One is defined with the film initially set in a single domain state and the bias field increased from zero to a saturation value. The other characteristic results from the field decreased from saturation back to zero.

By integrating the X_{jj} function the result is the average normalized static component of $\vec{M}$ parallel to the j axis as a function of H_j. This is true of either the increasing or decreasing characteristic. As shown by Equation 4, an alternative representation of this component is the average cosine of some angle. As an example, consider $j = 90^o$ where this angle, φ_{90}, has three different interpretations, depending on the dc field value and the field history of the film. The first interpretation concerns the increasing characteristic for fields from zero to values less than H_k, where φ_{90} is the angle between the mean direction of $\vec{M}$ and the average hard axis (HA). This interpretation is not very accurate for high dispersion films and will be discussed in Section B. For fields greater than H_k, to $H_j = \infty$, where the mean direction of $\vec{M}$ is parallel to the 90^o axis, the angle is that between the local $\vec{M}$ and the HA, or the local ripple angle. For field values less than H_k, when the film is composed of

splitting or strip domains, the angle is that between the mean direction of the magnetization in one domain and the average HA.

In all cases the integration was done by manually finding the area under the X_{jj} - H_j curve for a sufficient number of H_j values.

This part of the thesis is specifically concerned with the decreasing characteristic for j = 0°, 45°, and 90°. The dc field path is defined by the straight line oriented j degrees from the original easy direction and tangential to the switching asteroid. The zero field point is the point of tangency. It has been said (31, 35) that if the field is swept from saturation values back towards the asteroid the mean direction of $\vec{M}$ is parallel to the field (j) axis, which means that φ_j represents the local ripple angle. These ideas are illustrated in Figure 1b and will be discussed in more detail shortly.

As seen by Equation 4 the result of the measurements and subsequent integration is the quantity $\overline{\cos\varphi_j}$. What is desired is a measure of $\overline{\varphi_j(H_j)}$. Consider that the distribution of angles describing the ripple structure basically resembles a sinusoid and that φ_j (a measure of the local direction of $\vec{M}$) oscillates equally about the j axis between two equal maximum values, $\pm\varphi_{max}$ (bimodal angular distribution). If this is the case it can be shown that if $\bar{\varphi}$ (the average rms value of φ and equal to $\varphi_{max}/\sqrt{2}$) is less than about 20°, a very good approximation would be that $\overline{\cos\varphi_j} \simeq \cos\bar{\varphi}_j$. Henceforth $\bar{\varphi}_j$ will be called just the rms value of φ_j or the ripple angle or ripple amplitude.

The fact that integration of the decreasing X_{jj} curve is permissible is confirmed by a comparison of the magnitude of the real and imaginary

parts of X_{jj}. These are seen in Figures 4 and 5 for $X_{90,90}$ for samples 5Ba and II. The only region on the field axis where loss is more than just discernible is around H_k on the increasing curve for sample 5Ba, and from zero to about H_k on the curve for sample II. So there's no problem in integrating the decreasing curves in either film. Integration of the increasing curve will be discussed next.

To get a value of M (saturation magnetization) to conveniently effect normalization in Equation 4, two fundamental techniques are available. The method most commensurate with the integration procedure is to consider the lower limits in the integrals of Equation 3 and the increasing characteristic for $X'_{90,90}$, Figures 4 and 5. For this curve, $M_{90} = 0$ at $H_{90} = 0$. So the entire area under the increasing $X'_{90,90}$ curve is equivalent to M, provided first of all that the loss component is negligible. As seen by the curves the area under the $X''_{90,90}$ curves is a negligible perturbation compared to the area under the corresponding real part. So a very good approximation would be to neglect this loss effect. Obviously a more exact value would be the area under the $|X' - jX''|_{90,90}$ curve. A second qualification of this technique is that it is accurate only for low dispersion films. The reason is that the measured $X'_{90,90}$ curve and its integral do not take into account irreversible flux changes (partial switching) which are a function of the bias field H_{90}. Flux variations such as these seem to be more prevalent in the higher dispersion films where, according to Cohen (19, 20), the partial switching is due to the partial rotation phenomenon.

The other method of obtaining a value of M is to use the expression $M = H_k |X_{90,90}(H_{90} = 0)|_{\text{increasing curve}}$. This technique must also be

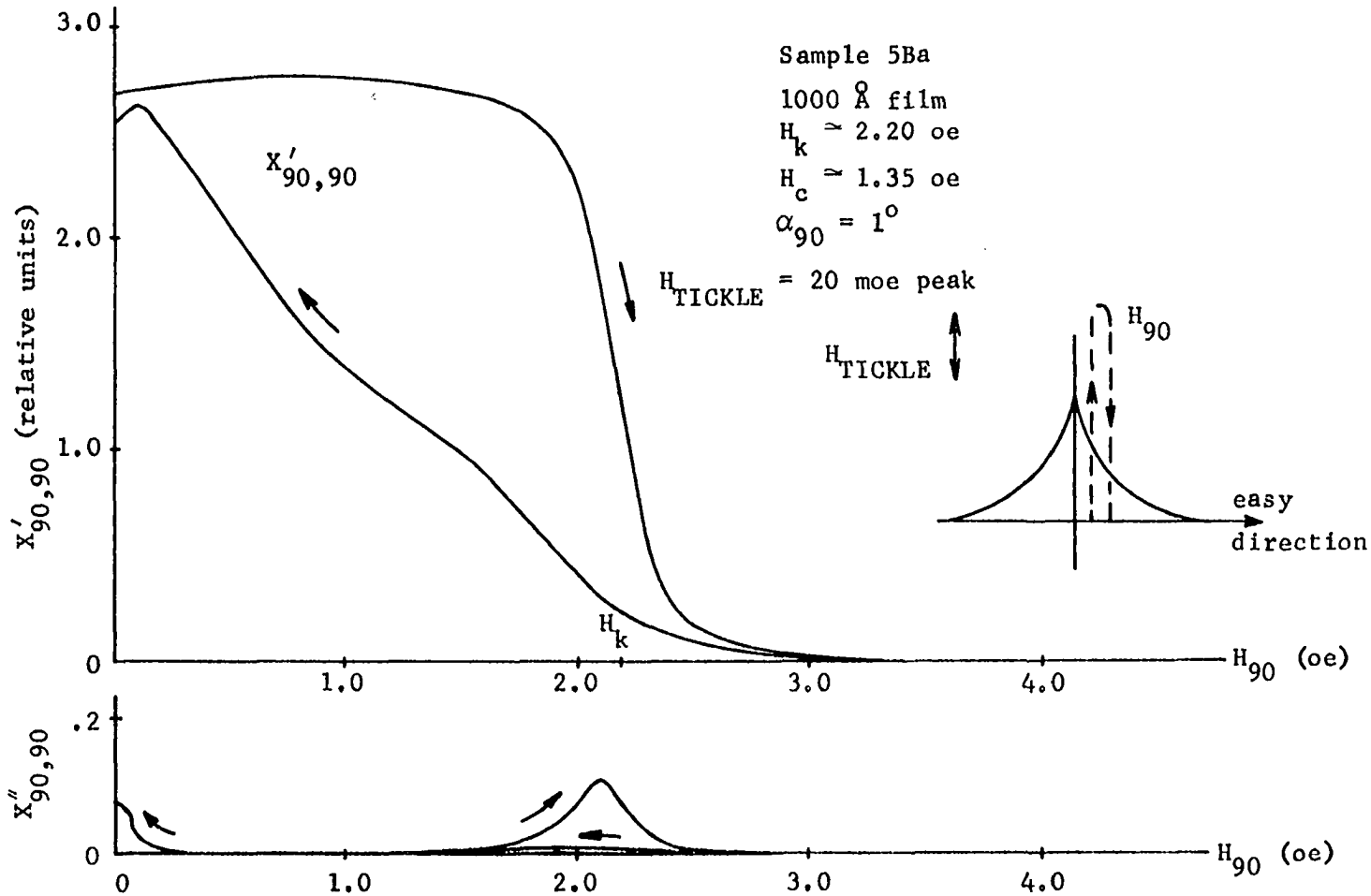

Figure 4. Real ($X'_{90,90}$) and imaginary ($X''_{90,90}$) parts of $X_{90,90}$ versus H_{90}. Note the ordinate scale of $X''_{90,90}$ is 3.2 times that of $X'_{90,90}$

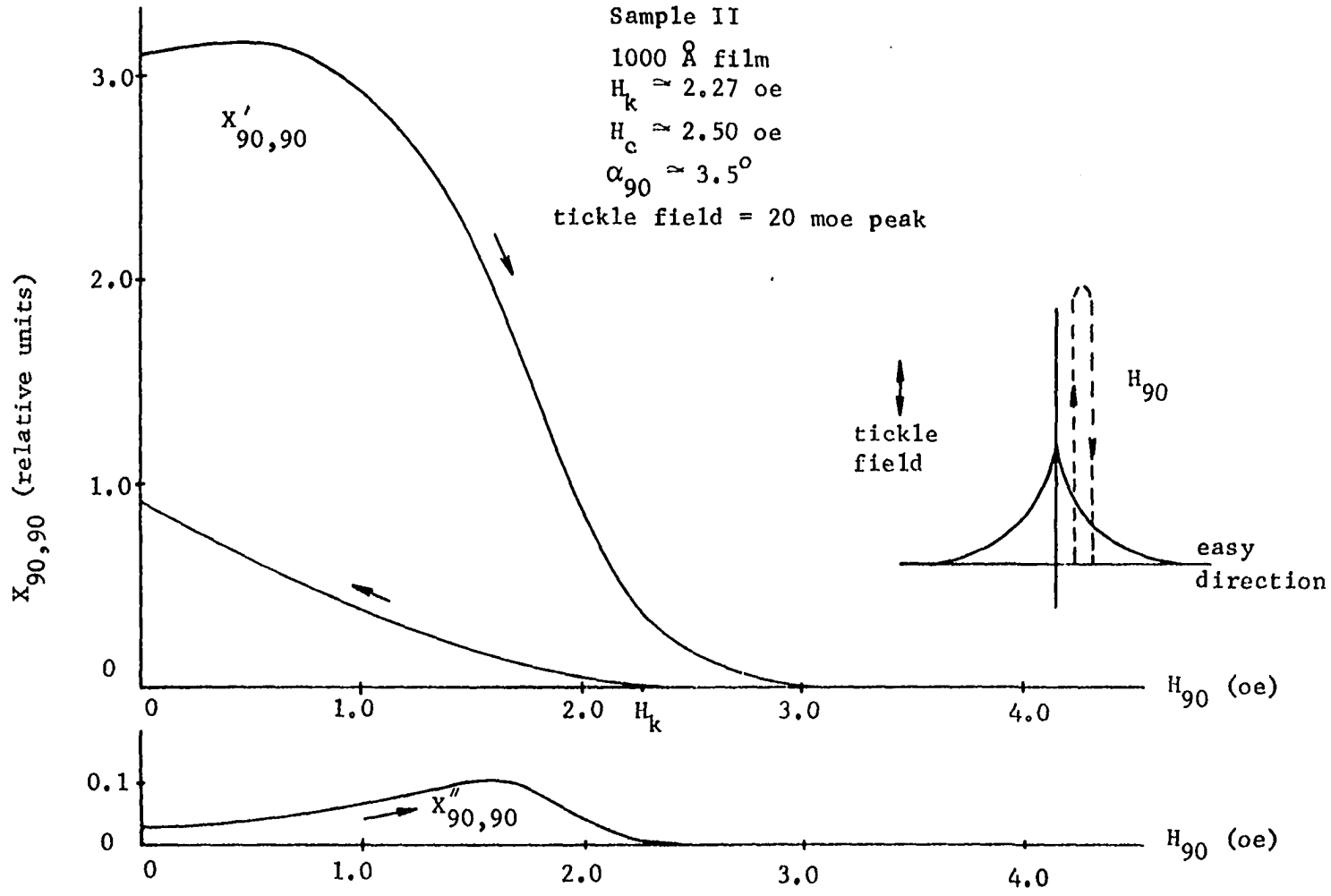

Figure 5. Real ($X'_{90,90}$) and imaginary ($X''_{90,90}$) parts of $X_{90,90}$ versus H_{90}. The ordinate scale of $X''_{90,90}$ is 3.2 times that of $X_{90,90}$

used with care since its accuracy is affected by any ripple pinning which might be present. Sample II exhibits pinning at $H_{90} = 0$, as seen by the low field loss on the $X''_{90,90}$ curve of Figure 5. Pinning causes a lower $X'_{90,90}$ than would otherwise be the case and the effect can be compensated for by increasing the measured $X'_{90,90}$ at $H_{90} = 0$ to the value obtained by extrapolating the linear function $(X'_{90,0})^{-1}$ vs H_0 back to $H_0 = 0$. The values of $\bar{\varphi}_j$ in this report were computed using this technique for finding M.

Figure 6a shows the curves of $X'_{0,0}$ for the two samples. The loss component was not recorded but was observed to be negligible until wall switching was initiated. This characteristic did not extend for a very large field interval for sample 5Ba since this film switched by wall motion before much output was realized. Sample II was sufficiently dispersed ($\frac{H_c}{H_k} = 1.1$ for sample II versus 0.614 for sample 5Ba) that wall switching was inhibited and meaningful output was obtained for a larger field interval. The tickle field was increased from 20moe to 75 (or 100) moe for these curves to get as much output as possible.

Figure 6b shows $X'_{45,45}$ for samples II and 5Ba. These characteristics also were low in measurable loss in the region of interest.

The resulting curves of $\bar{\varphi}_j$ are plotted in Figure 7 together with a theoretical curve of Hoffmann (22, 23) for $\bar{\varphi}_{90}$. This shows the fairly close agreement between the present experimental approach and pure theory. The theoretical curve came from the expression (23)

$$\bar{\varphi}_{90} = (\text{constant})(H_{90} - H_k)^{-3/8} \qquad (5)$$

The constant was evaluated at the point of intersection between this curve and the $\bar{\varphi}_{90}$ curve of sample 5Ba, as seen in Figure 7. More will be said

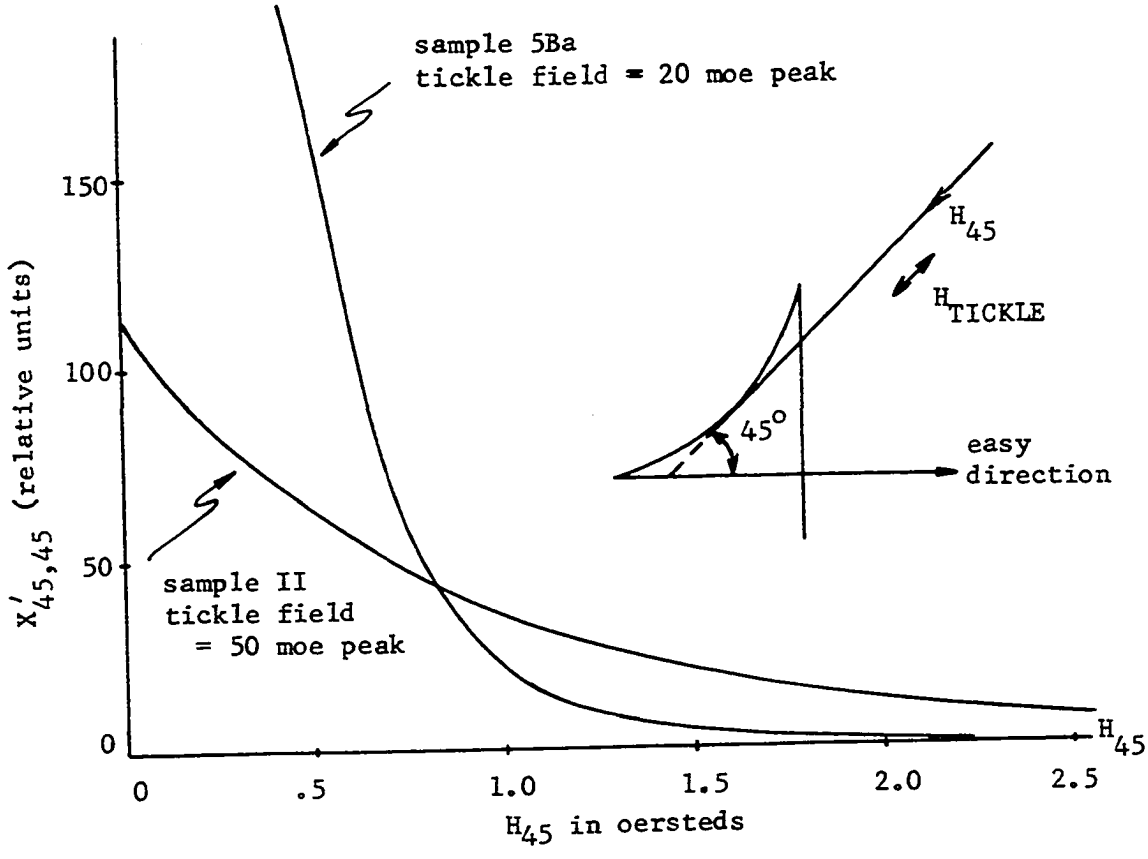

Figure 6a. $X'_{45,45}$ versus H_{45} for two samples

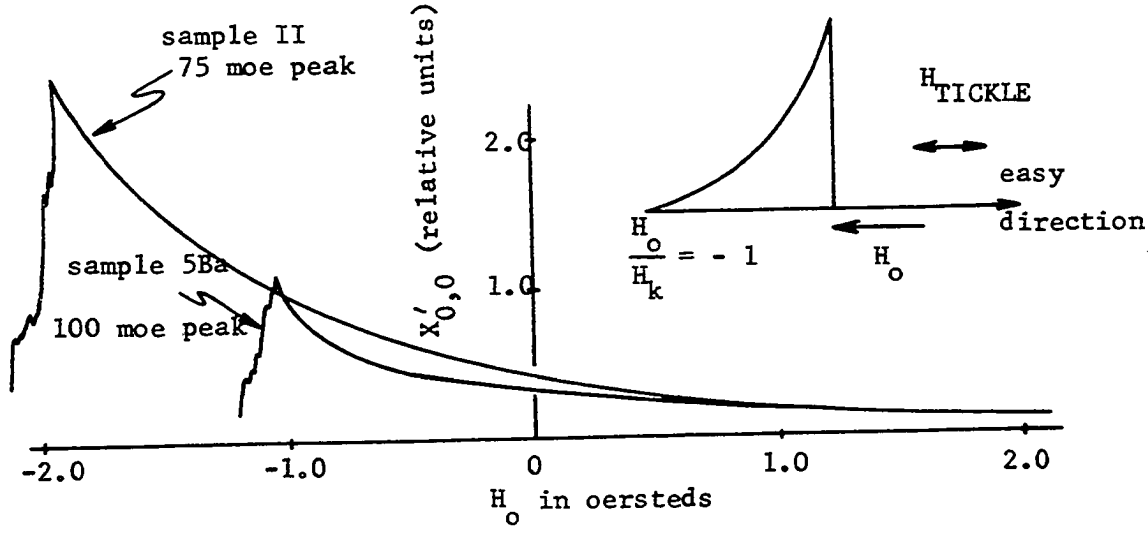

Figure 6b. $X'_{0,0}$ versus H_0 for two samples

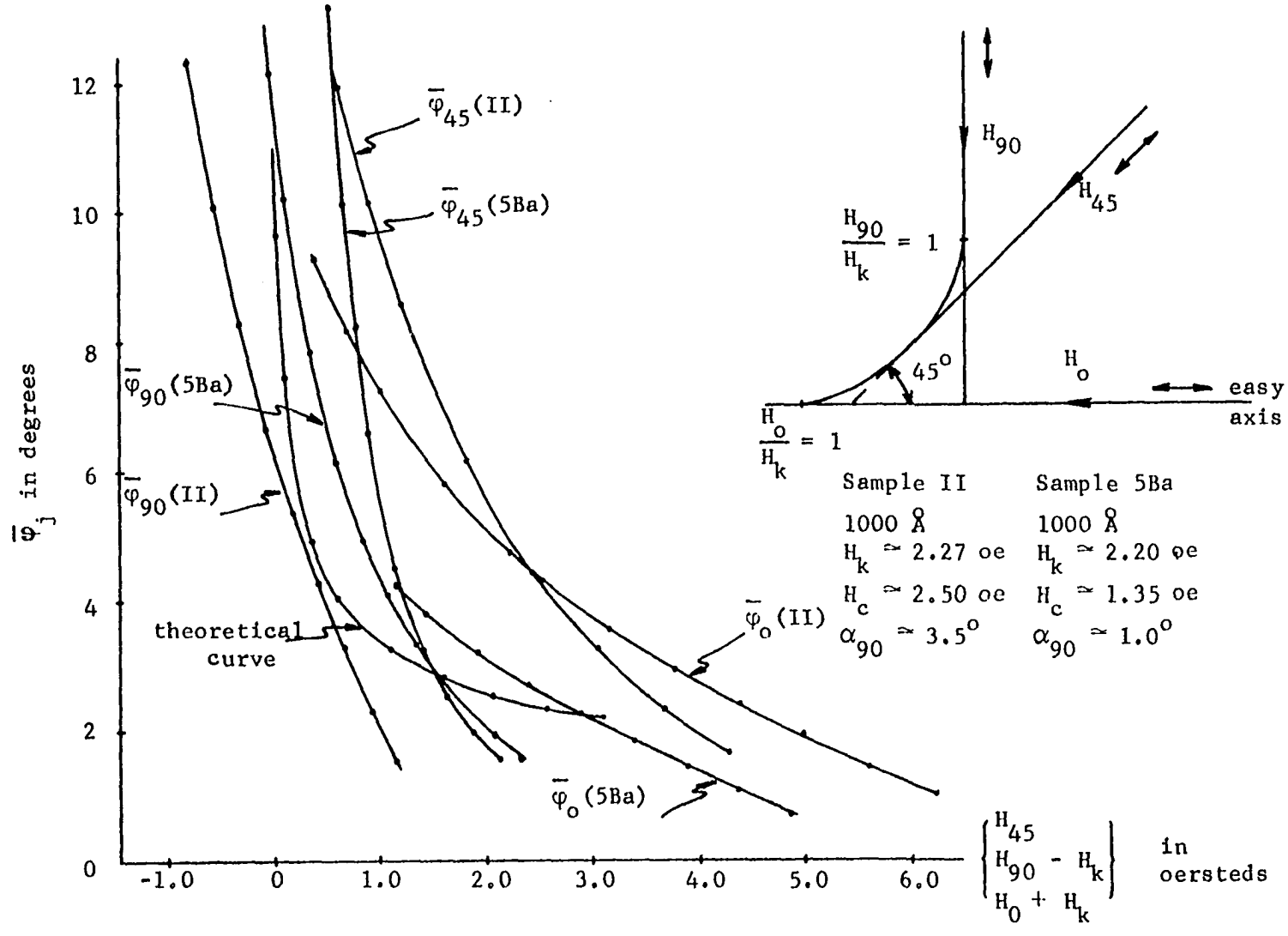

Figure 7. RMS ripple angle versus respective orienting field

about this curve in Section F. Note the curves are plotted with the respective zero field points being the points of tangency with the asteroid, or where the field path goes theoretically unstable. This means the field values on the graph are $(H_0 + H_k)$, H_{45}, and $(H_{90} - H_k)$ for $\bar{\varphi}_0$, $\bar{\varphi}_{45}$, and $\bar{\varphi}_{90}$ respectively.

The curves are perhaps more separated than was hoped they would be. $\bar{\varphi}_0$ and $\bar{\varphi}_{90}$ for sample 5Ba are in fairly close agreement but the same two for sample II are considerably separated. One explanation for this lies in integration (operator) errors. For the relatively low and noisy output signals at the higher pertinent field values $(H > H_k)$ it was difficult to effect accurate area measurements. For lower field values, where the integration was less of a problem, nonlinearities, stray fields, and ripple amplitudes became large, which approached invalidation of some of some of the mathematical approximations. As the field decreased, these effects would accentuate any differences in the ripple structures for the two different bias field conditions.

The fact that the $\bar{\varphi}_{45}$ curves rise so steeply, and cross the respective $\bar{\varphi}_0$ curves, as H_{45} decreases can be explained by the action of the uniaxial anisotropy forces. Assume for large fields that the ripple structure can be described by parallel bands of magnetization whose rms direction alternates about the field axis from band to band, as seen in Figure 1a. Under ideal conditions, for any tangential field path other than 0°, 45°, and 90°, the anisotropy forces are not symmetrical about that axis. The reason for this is the torque goes as $\sin 2\theta$, where θ is the angle between the rms direction of $\vec{M}$ in a band and the ED. θ is different for two adjacent bands which in general results in unequal torques on the

respective magnetizations (as seen by θ_+ in Figure 1a). As the bias field approaches the asteroid on its tangential path the wavelength and amplitude of the ripple increase, which leads to an increase in the effect of the anisotropy torques. From Figure 1a, the band of $\bar{\varphi}_{j+}$ would experience a greater torque than the $\bar{\varphi}_{j-}$ band, if j were greater than 45°. This would tend to cause $\bar{\varphi}_{j+}$ to become larger than $\bar{\varphi}_{j-}$. This leads to induced demagnetizing fields and the possible resultant rotation of the whole structure. This in turn results in a larger net component of $\vec{M}$ perpendicular to the tickle field which causes an increased output and an increased effective $\bar{\varphi}_{45}$. Hoffmann (23) discussed this increase in amplitude and wavelength for a decreasing 90° bias field. It led to ripple instability and his "blocked state". The process described above is similar but occurs at a higher field magnitude.

What all this says is that the ripple structure is probably the same for all field orientations provided the fields are sufficiently large. However, as the field point approaches the asteroid and the net local forces relax, the unsymmetrical forces can become dominant and give rise to apparent anomalous results. This also says the 45° field path orientation in the present experiment wasn't exactly aligned.

B. Calculation of Internal Fields in a Splitting Domain Structure

This section involves an extension of Equation 4 where it was shown that the average component of $\vec{M}$ parallel to the j axis, $\bar{M}_j$, is proportional to the area under the $\bar{X}_{jj}(H_j)$ curve from $H_j = \infty$ to $H_j = H_j$. Consider j = 90° and from Equation 4,

$$\frac{\bar{M}}{M}90 = \overline{\cos\varphi_{90}} = \overline{\sin\phi_+(H_{90})} \tag{6}$$

In Equation 6 $\overline{\phi_+}$ is the compliment of $\bar{\varphi}_{90}$. It also has three interpretations depending on the value of H_{90} and how that value was approached. For a single domain film and $H_{90} < H_k$, $\bar{\phi}_+$ will be taken to mean the average angle between the mean direction of $\vec{M}$ and the easy direction. As mentioned in the last section this interpretation is not very accurate for highly dispersed samples and will be discussed in detail shortly. When the mean direction of $\vec{M}$ coincides with the HA, as when H_{90} is decreased from a saturation value, $\bar{\phi}_+$ is interpreted as the average angle between the mean direction of $\vec{M}$ in a strip domain (for $H_{90} < H_k$), or the average rms direction of $\vec{M}$ in a ripple band (for $H_{90} > H_k$), and the original (+) easy direction. $\bar{\phi}_+$ is always less than 90°. Assuming the film samples under consideration are free of very long wavelength magnetization variations and skew, no problem exists in assuming that

$$\overline{\sin\phi_+} \simeq \sin\bar{\phi}_+ \tag{7}$$

for single domain configurations. From the observed parallel nature of splitting or strip domains and the relative uniformity of the magnetization within (17, 20) it will be assumed that Equation 7 is a good approximation for that type of structure also.

$\bar{\phi}_+$ then has a single interpretation for three different structures. Its meaning is ambiguous for combined structures around transition field intervals, e.g. for the increasing characteristic where $.7H_k < H_{90} < H_k$.

For convenience another angle will be introduced for discussion of

the splitting domain structure and its bimodal angular distribution. Consider $\bar{\phi}_-$ to be the average angle between the opposite ED and the mean direction of $\vec{M}$ in strip domains which have a component antiparallel to the original ED. Note $|\bar{\phi}_+| \cong |\bar{\phi}_-|$.

$\frac{\bar{M}}{M}_{90}$ versus H_{90} is plotted for the two samples for both the increasing and decreasing characteristics and are seen in Figure 8. The curves for sample 5Ba for the field intervals involved are fairly representative of the macroscopic M-H characteristic commonly observed. The ordinate is equal to $\sin\bar{\phi}_+$ only up to approximately $H_{90} \simeq .9H_k$ for sample 5Ba. For higher values of H_{90} the angle loses its meaning.

$\bar{\phi}_+$ versus a normalized H_{90} is plotted in Figure 9 for both samples. Again, for values of $H_{90} \gtrsim .9H_k$ in regards to sample 5Ba, the interpretation of $\bar{\phi}_+$ is ambiguous. The theoretical curve of Stoner-Wohlfarth (1) is also plotted for comparison and it is interesting to note the large angle to which experimental data of 5Ba agrees quite closely with the single domain coherent rotation model. Also of interest is the $\Delta\bar{\phi}_+$ separation between the single domain and strip domain structures. This shows the effect of the fields from the splitting domain walls forcing $\vec{M}$ within the domains to larger values of $\bar{\phi}_+$. The remanent (at $H_{90} = 0$) $\bar{\phi}_+$ and $\Delta\bar{M}_{90}$ (Figures 8 and 9) for sample II are considerably larger than those of sample 5Ba which demonstrates the higher wall energy and fields of this sample. Hoffmann (22) points out that the larger grain size results in a finer splitting-domain structure which in turn causes larger wall fields.

The increasing $\frac{\bar{M}}{M}_{90}$ and $\bar{\phi}_+$ curves for sample II are only indications

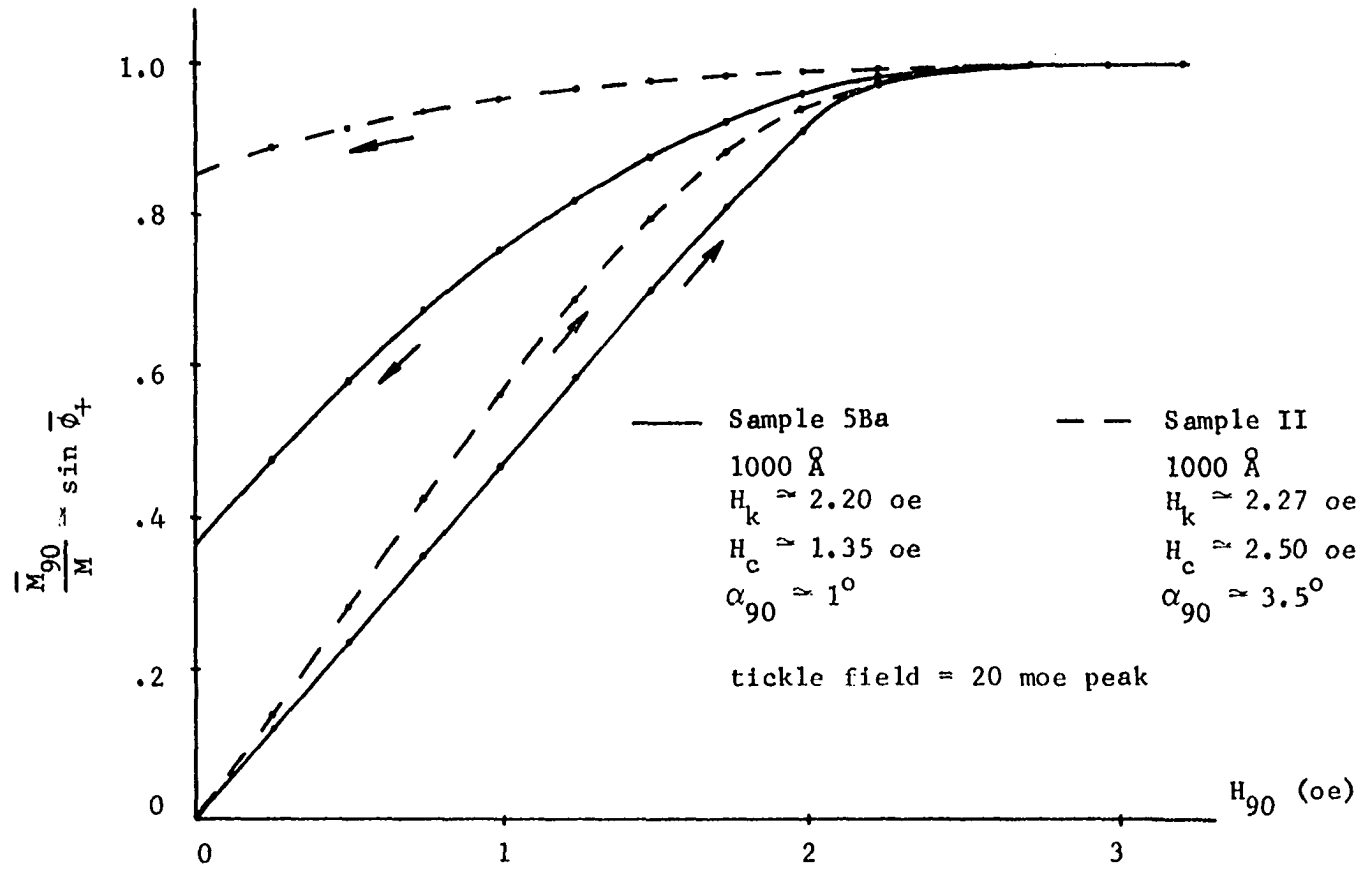

Figure 8. Measured values of $\bar{M}_{90}/M$ versus H_{90}

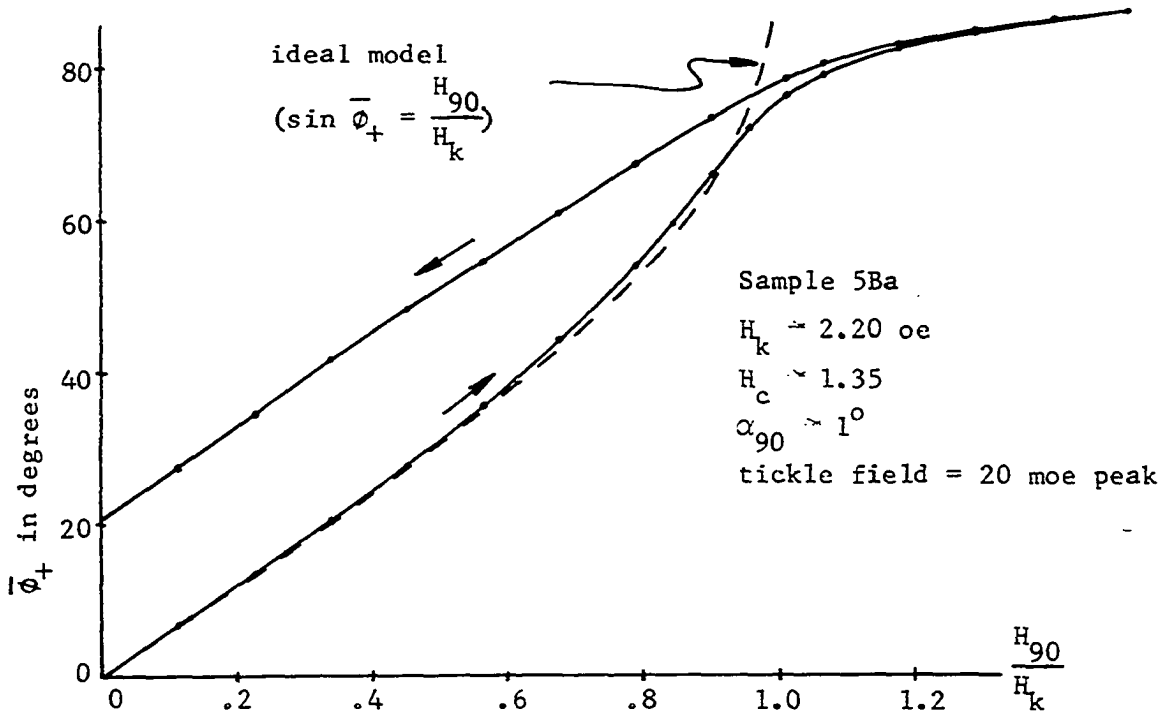

Figure 9a. Measured and ideal single domain values of $\bar{\phi}_+$ versus H_{90}/H_k for sample 5Ba

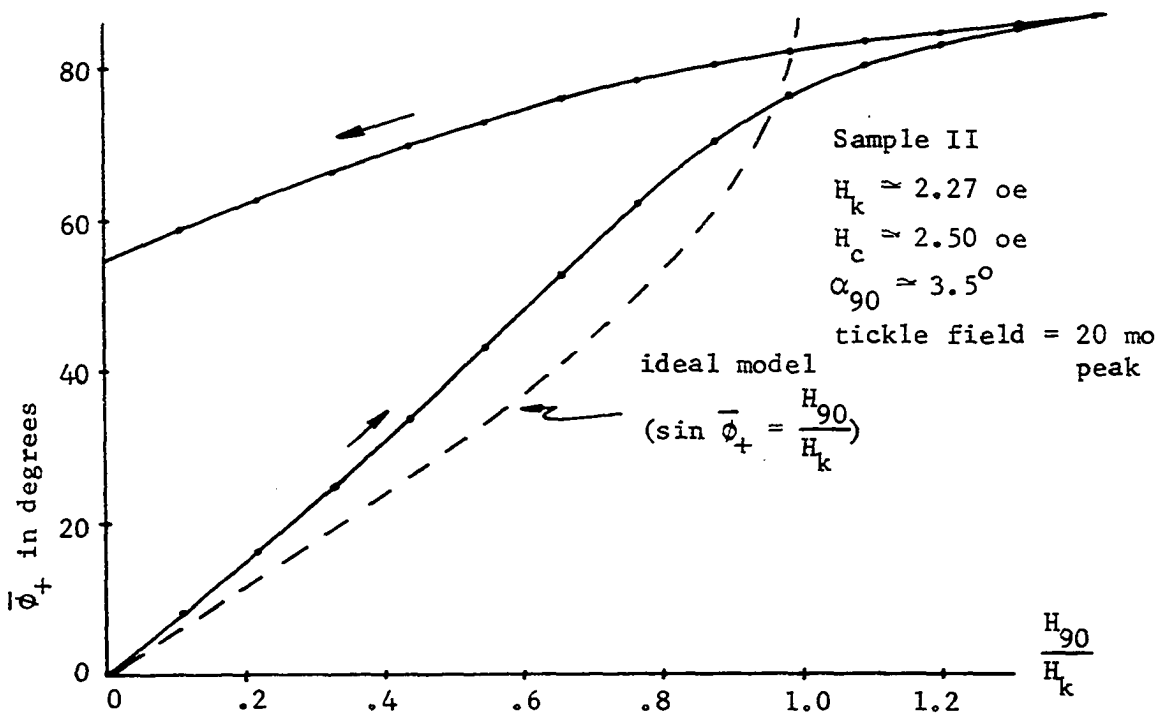

Figure 9b. Measured and ideal single domain values of $\bar{\phi}_+$ versus H_{90}/H_k for sample II

of the actual processes taking place and not an accurate measure of the quantities involved. These curves as well as the value of M, mentioned in the last chapter, are based upon the increasing $X'_{90,90}$ curve. This curve, for sample II, has an inherent problem and will be discussed next.

Consider a film in a single domain state and H_{90} increasing from zero. The mean $\vec{M}$ will rotate into the field direction. Under ideal single domain conditions the slope of the resulting macroscopic M_{90} - H_{90} curve would be constant out to $H_{90} = H_k$. However, real films deviate from this behavior in that they experience partial switching before H_k is reached. Whether the partial switching process represents a large difference between the ideal and measured curves is dependent on the dispersion characteristics of the film. According to Cohen (19) in this region of field space high dispersion films experience partial rotation while low dispersion films experience edge or labyrinth domain propagation. In the high dispersion sample II of this investigation it is believed that both processes occur. The reason is that $X''_{0,90}$ (Figure 10) is observed for low values of H_{90}, which is interpreted as labyrinth domain wall rearrangements. Note that no $X''_{0,90}$ loss exists for low values of H_{90} for sample 5Ba, as seen in Figure 11. Sample II deviates considerably from the ideal case, as seen by the $X_{90,90}$ curves in Figure 5 and $\sin\bar{\phi}_+$ and $\bar{\phi}_+$ vs H_{90} in Figures 8 and 9. An explanation lies in the fact that rapid irreversible magnetization rotations (partial switching) are taking place as a function of the dc field and not the tickle field. This means that these flux changes are not picked up by the measuring technique. It results in a smaller component of $\vec{M}$ perpendicular to the tickle field and stray field locking.

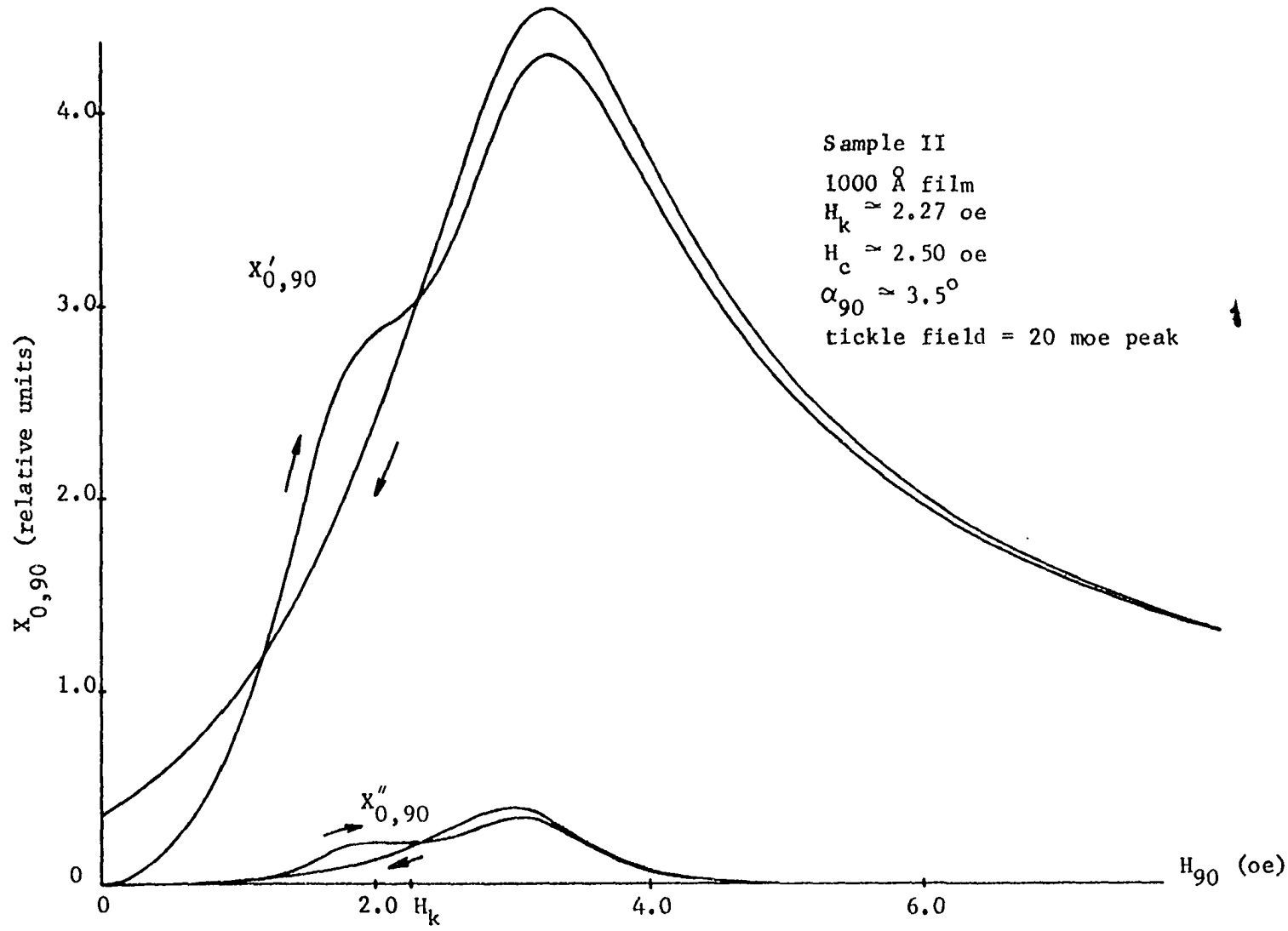

Figure 10. Real ($X'_{0,90}$) and imaginary ($X''_{0,90}$) parts of $X_{0,90}$ versus H_{90}

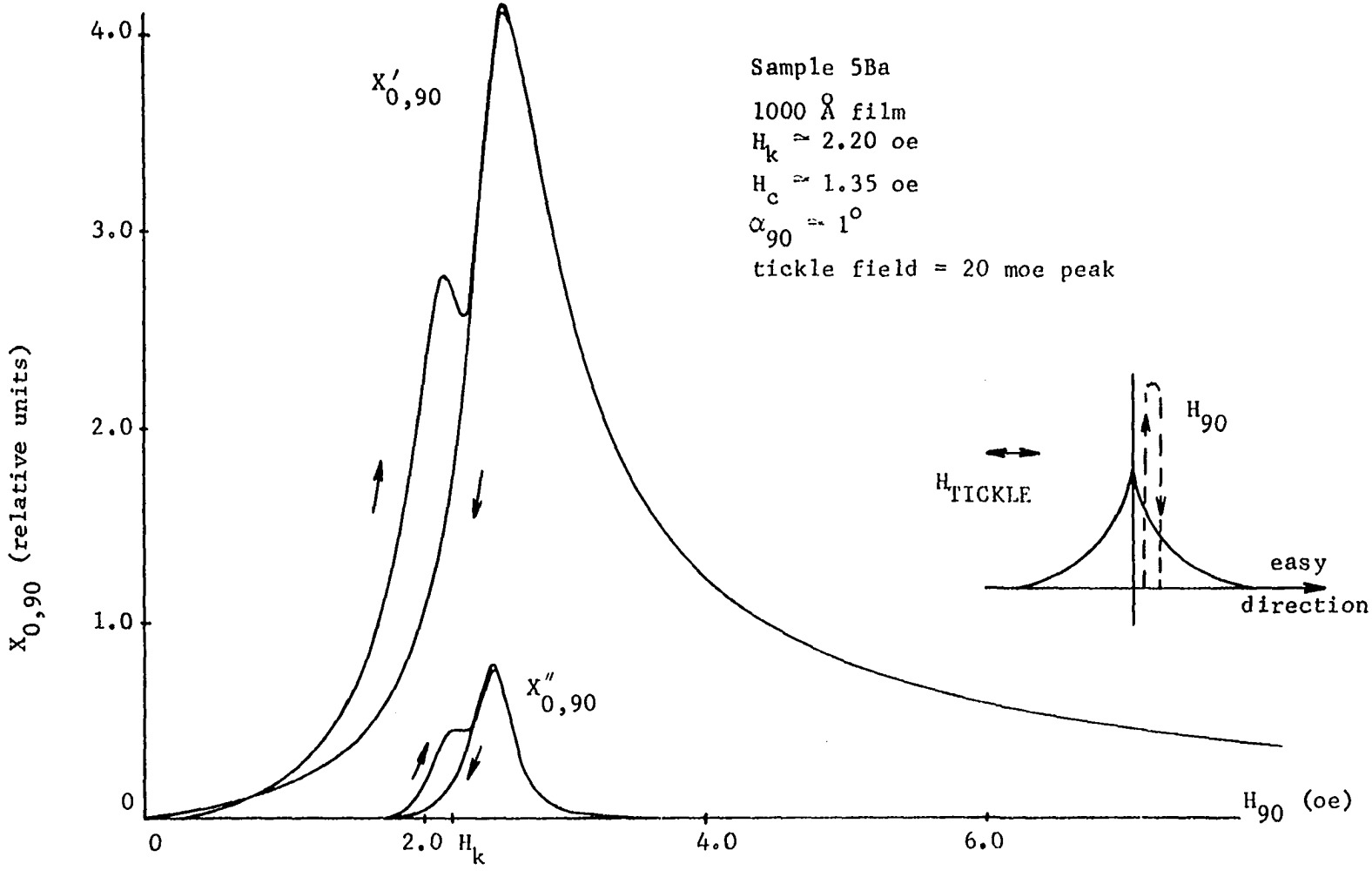

Figure 11. Real ($X'_{0,90}$) and imaginary ($X''_{0,90}$) parts of $X_{0,90}$ versus H_{90}

If only an indication this point is seen by Figure 9 where the values of $\bar{\phi}_+$ for low field values are larger than the comparative ones of sample 5Ba. This again points to the existence of switched portions in the film. The combination of these effects causes smaller measured values of $\overline{\Delta M}_{90}$ and $\bar{X}'_{90,90}$ than would otherwise be the case. This other case is seen by sample 5Ba, in Figure 4, where the $X'_{90,90}$ curve is more of a constant function of H_{90}. If this film partially switches by edge domain propagation, it does so slowly enough that most of the flux changes are measured through the action of the tickle field. These effects are seen in a cumulative sense by the area under the increasing $X'_{90,90} - H_{90}$ curve. For the ideal single domain model this area would be the product of $X'_{90,90}$ at $H_{90} = 0$ and H_k. The actual area under the measured curve was 30% less than this for sample II and 2% less for sample 5Ba. These figures include small corrections for ripple pinning at $H_{90} = 0$.

In this investigation, the technique used to obtain a measure of M for $\bar{M}_{90}/M$ as plotted in Figure 8 was the area under the $X'_{90,90}$ curve. The process used to obtain the return characteristics of $\bar{\phi}_+$ vs H_{90} and the ripple angle $\bar{\varphi}_j$ of Section A was the product $H_k X'_{90,90}(0)$. The angle $\bar{\phi}_+$ will be used in the internal field calculations which will be described next.

Assume the film is saturated in the average hard direction and H_{90} is then decreased to a value less than H_k. The film is now in a strip domain configuration. Assume that for a given applied H_{90}, and zero tickle field, the magnetization in half the strip domains lies at an average equilibrium angle of $\bar{\phi}_+$ with respect to the inital ED, and the other half at an angle of $\bar{\phi}_-$ with respect to the antiparallel ED. The average

static torques which are $\bar{\phi}_+$ dependent, acting on the magnetization in approximately the center of a given $\bar{\phi}_+$ strip domain, can be arbitrarily broken up as follows:

$$\bar{T}_0(\bar{\phi}_+),\ \bar{T}_{wall}(\bar{\phi}_+),\ \bar{T}_{local}(\bar{\phi}_+),\ \bar{T}_{shape}(\bar{\phi}_+),\ \text{and}\ \bar{T}_{demag}(\bar{\phi}_+).$$

The first torque is due to the uniaxial anisotropy and the applied dc field. The second comes about from the average effect of magnetostatic, exchange, and uniaxial anisotropy energies in the walls. The third, an average local torque which is of microscopic origin (8, 22), includes contributions from magnetocrystalline and/or strain-magnetostriction anisotropies, chemical and spacial inhomogeneities, and exchange effects. These terms, which contribute to the cause of ripple, can give rise to distributed volume magnetization divergences and resulting stray fields. If the ripple amplitude becomes large, these fields can become appreciable. The shape torque contribution comes from the shape anisotropy of the film sample. The last torque is due to the discontinuity of the normal component of $\vec{M}$ across walls.

Figure 12 represents a simplified strip domain structure which shows what happens to the mean magnetization within the domains under the influence of a tickle field applied either parallel to the EA (Figure 12a) or the HA (Figure 12b). For the case of an EA tickle, assuming the domain walls are pinned (not free to rotate), it is seen that $\vec{M}$ will assume a new position, slightly displaced from its original orientation, defined by $\bar{\phi}_1 = \bar{\phi}_+ + \overline{\delta\phi}$ in the domains with an increased component of $\vec{M}$ normal to the EA walls. Also $\bar{\phi}_2 = \bar{\phi}_- - \overline{\delta\phi}$ for domains oriented in the opposite direction with a diminished normal component. It is seen that there is a discontinuity

Figure 12a. Simplified strip domain structure showing EA and HA walls, angles used in text, and dominant demagnetizing fields for an EA tickle field

Figure 12b. Simplified strip domain structure showing EA and HA walls, angles used in text, and dominant demagnetizing fields for hard axis tickle field

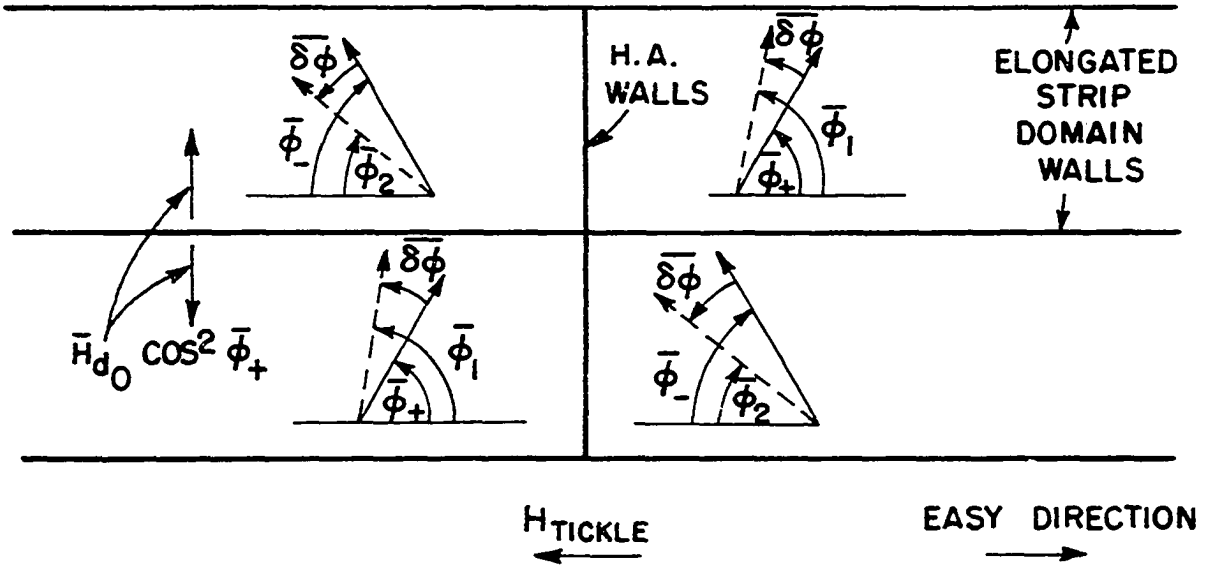
H.A.
WALLS
ELONGATED
STRIP
DOMAIN
WALLS
$\bar{H}_{d_0} \cos^2 \bar{\phi}_+$
H_{TICKLE}
EASY DIRECTION

(a)

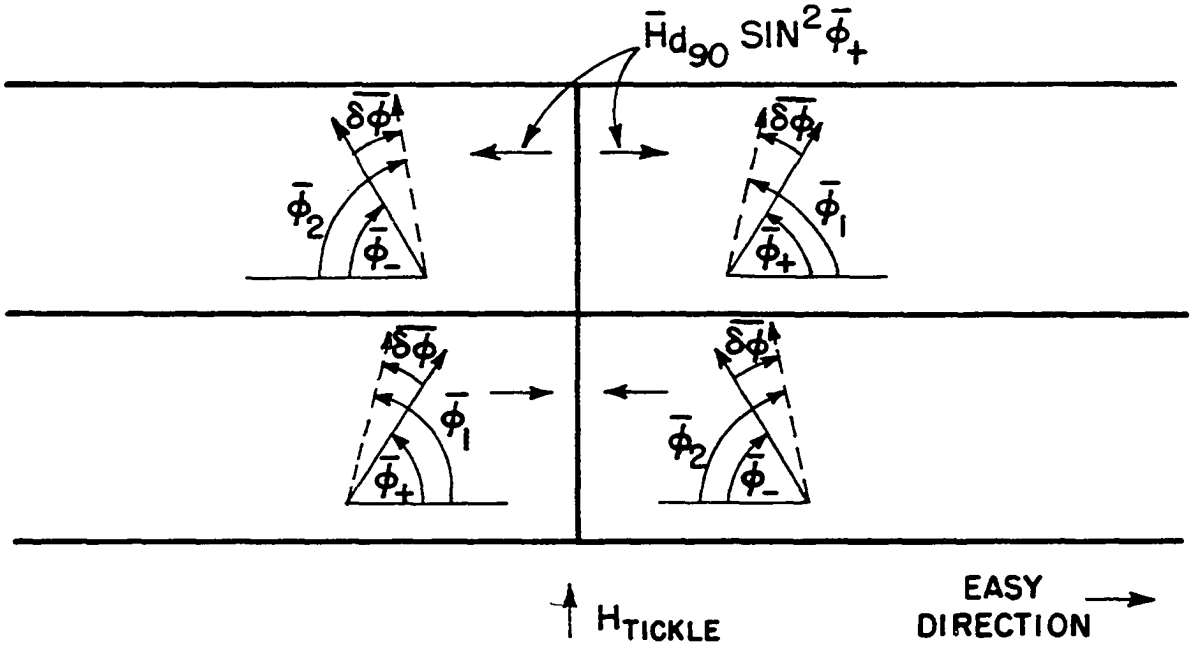
$\bar{H}_{d_{90}} \sin^2 \bar{\phi}_+$
H_{TICKLE}
EASY
DIRECTION

(b)

in the normal component of $\vec{M}$ across the EA walls giving rise to a demagnetizing field which opposes the effect of the applied tickle field. The demagnetizing field contribution from walls parallel to the HA for an EA tickle field are essentially zero because the average net discontinuity in the normal component of $\vec{M}$ does not significantly change. Note also that the induced demagnetizing fields from HA walls for a HA oriented tickle field are much, much smaller than the fields from EA walls due to an EA tickle. As seen in Figure 12 this is due to the very elongated domains, and the fact that the field from the magnetic pole density induced on two adjacent HA walls could be considered a dipole field which drops off very rapidly and is very small near the center of a domain. These demagnetizing fields only occur if the small angle strip domain walls are pinned. If the walls rotated to a new position, they could completely cancel the discontinuity in $\vec{M}$.

Assume $\overline{\delta\phi}$ is sufficiently small that the torques can be expanded about the zero tickle field orientation, $\bar{\phi}_+$, and that a first order approximation is of sufficient accuracy. Then, for a $\bar{\phi}_1$ domain,

$$
\begin{aligned}
\bar{T}_0(\bar{\phi}_1) &\simeq \bar{T}_0(\bar{\phi}_+) + M\,\overline{\delta\phi}(H_k \cos 2\bar{\phi}_+ + H_{90} \sin\bar{\phi}_+) \\
\bar{T}_{wall}(\bar{\phi}_1) &\simeq M\bar{H}_w(\bar{\phi}_+) + M\bar{H}^*_w(\bar{\phi}_+)\overline{\delta\phi} \\
\bar{T}_{local}(\bar{\phi}_1) &\simeq M\bar{H}_l(\bar{\phi}_+) + M\bar{H}^*_l(\bar{\phi}_+)\overline{\delta\phi} \\
\bar{T}_{shape}(\bar{\phi}_1) &\simeq M\bar{H}_s(\bar{\phi}_+) + M\bar{H}^*_s(\bar{\phi}_+)\overline{\delta\phi} \\
\bar{T}_{demag}(\bar{\phi}_1) &\simeq (M\bar{H}_{d_o} \cos^2\bar{\phi}_+ + M\bar{H}_{d_{90}} \sin^2\bar{\phi}_+)\overline{\delta\phi}
\end{aligned}
\tag{8}
$$

The (*) stands for differentiation with respect to ϕ. The last torque, from induced demagnetizing fields, $\bar{H}_d$, brought about by the tickle field, has only one effective term in it. The other term is negligible depending

along which axis the tickle field is applied. The $\bar{H}_{d_o}$ term predominates for an EA tickle and $\bar{H}_{d90}$ for a HA tickle field. The EA term, with a similar argument for the HA term, can be derived by assuming that $\bar{H}_d$ was proportional to the difference in the normal components of $\vec{M}$ from the center of one strip domain to the center of an adjacent one, i.e.

$$\begin{aligned} H_d(\bar{\phi}_1) &= (\text{const})[\sin(\bar{\phi}_+ + \overline{\delta\phi}) - \sin(\bar{\phi}_+ - \overline{\delta\phi})] \\ &\simeq H_{d_o}\, \overline{\delta\phi}\, \cos\bar{\phi}_+ \end{aligned} \tag{9}$$

neglecting the $\overline{\delta\phi^2}$ term gives

$$\begin{aligned} \bar{T}_{demag}(\bar{\phi}_1) &= M\overline{H_d}(\bar{\phi}_1)\, \cos(\bar{\phi}_+ + \overline{\delta\phi}) \\ &\simeq M\, \overline{H_{d_o}}\, \overline{\delta\phi}\, \cos^2\bar{\phi}_+ \end{aligned} \tag{10}$$

The sum of the net restoring torques has to equal the torque $\overline{\Delta T_o}$ due to the EA tickle field, ΔH_o, which caused the displacement of $\vec{M}$ from its $\bar{\phi}_+$ equilibrium position. This gives

$$\begin{aligned} \overline{\Delta T_o} &= \bar{T}(\bar{\phi}_1) - \bar{T}(\bar{\phi}_+) \\ &\simeq M\overline{\delta\phi}[H_k \cos 2\bar{\phi}_+ + H_{90} \sin\bar{\phi}_+ + \bar{H}_0^*(\bar{\phi}_+)] \end{aligned} \tag{11}$$

where $\bar{H}_0^*(\bar{\phi}_+) = \bar{H}_{s_o}^*(\bar{\phi}_+) + \bar{H}_{w_0}^* + \bar{H}_{1_o}^* + \bar{H}_{d_o}\cos^2\bar{\phi}_+$

If $\bar{\phi}_+ \gg \overline{\delta\phi}$ the average torque from the EA tickle field on the magnetization in a $\bar{\phi}_+$ domain can be approximated by

$$\overline{\Delta T_o} \simeq \Delta H_o M \sin\bar{\phi}_+ \tag{12}$$

Consider next an expression for $X_{0,90}$, from Equation 1,

$$\bar{X}'_{0,90} = \frac{\overline{\Delta M_o}}{\Delta H_o}(H_{90}) \tag{13}$$

where $\overline{\Delta M_o(H_{90})}$ can be approximated by the expression $M\sin\bar{\phi}_+\overline{\delta\phi}$. The reason

for using the real part of $X_{0,90}$ in Equation 13 is that the field interval of interest does not have any significant loss in it. Combining Equations 11, 12 and 13 results in

$$\bar{X}'_{0,90} \simeq \left(\frac{M \sin^2\bar{\phi}_+}{H_k \cos 2\bar{\phi}_+ + H_{90}\sin\bar{\phi}_+ + \bar{H}^*_o(\bar{\phi}_+)}\right)_{avg} \tag{14}$$

In a similar fashion for the case of a tickle field applied parallel to the HA, Equation 1 gives

$$\bar{X}'_{90,90} = \frac{\overline{\Delta M_{90}}}{\Delta H_{90}} \simeq \frac{M\cos\bar{\phi}_+\overline{\delta\phi}}{\Delta H_{90}} \tag{15}$$

The torque balance is exactly analogous except for the demagnetizing fields from charges induced on the HA walls. There is negligible $\vec{\nabla}\cdot\vec{M}$ contributions across EA walls in this case. The torque from ΔH_{90} can be written as

$$\overline{\Delta T}_{90} \simeq \Delta H_{90} M\cos\bar{\phi}_+ \tag{16}$$

Equating Equation 16 to the net restoring torques and substituting into Equation 15 gives

$$\bar{X}'_{90,90} \simeq \left[\frac{M \cos^2\bar{\phi}_+}{H_k\cos 2\bar{\phi}_+ + H_{90}\sin\bar{\phi}_+ + \bar{H}^*_{90}(\bar{\phi}_+)}\right]_{avg} \tag{17}$$

where $\bar{H}^*_{90}(\bar{\phi}_+) = \bar{H}^*_{s_{90}}(\bar{\phi}_+) + \bar{H}^*_{w_{90}}(\bar{\phi}_+) + \bar{H}^*_{I_{90}}(\bar{\phi}_+) + \bar{H}_{d_{90}}\sin^2\bar{\phi}_+$

Expressions 14 and 17 can be modified for the case of a single domain structure by elimination of the wall and demagnetizing terms. It is believed that for films without large ripple amplitudes and relatively free of ripple pinning and large stray fields, the torque contribution from local fields, $M\bar{H}^*_I\,\overline{\delta\phi}$, due to the action of the tickle field, would be much smaller than that from the uniaxial anisotropy and applied field. This

being the case the $\bar{H}_1^*$ term can be neglected. From the size and shape of these two samples it can be assumed that the shape term can also be neglected. This results in

$$\bar{X}'_{0,90}(\text{S.D.}) \simeq \left(\frac{M\sin^2\bar{\phi}_+}{H_k\cos 2\bar{\phi}_+ + H_{90}\sin\bar{\phi}_+}\right)_{\text{avg}} \tag{18}$$

$$\bar{X}'_{90,90}(\text{S.D.}) \simeq \left(\frac{M\cos^2\bar{\phi}_+}{H_k\cos 2\bar{\phi}_+ + H_{90}\sin\bar{\phi}_+}\right)_{\text{avg}} \tag{19}$$

Using the measured values of $\bar{X}'_{0,90}$ and $\bar{X}'_{90,90}$, as seen in Figures 4, 5, 10, and 11, and normalizing them with respect to $\bar{X}'_{90,90}$ at $H_{90} = 0$ from the increasing characteristic; and using the computed values of $\bar{\phi}_+$, it is possible to solve for the internal fields in the expressions of Equations 14 and 17. These fields are plotted in Figure 13 as a function of $\bar{\phi}_+$. The curves show the approximate magnitude of the internal fields generated by the mechanisms described previously. It is seen that over a large range of $\bar{\phi}_+$ the internal fields generated when an EA tickle field is applied are considerably greater than those generated by a hard axis tickle. This is caused by the induced demagnetizing field contribution from walls parallel to the EA. It forms the major part of the total internal field. This is due to the fact that $\bar{H}^*_{w_0}$ is small because the net wall angle does not change appreciably. If the film is void of a gross ripple structure such that the ripple amplitude and stray fields are not large, then the local torque contribution, due to the action of the tickle field, is believed to be considerably smaller than the other terms and $\bar{H}_I^*$ can be neglected. So, neglecting $\bar{H}^*_{w_0}$ and $\bar{H}^*_{I_0}$ leaves only the shape term which can be discarded on the grounds that the film is round and

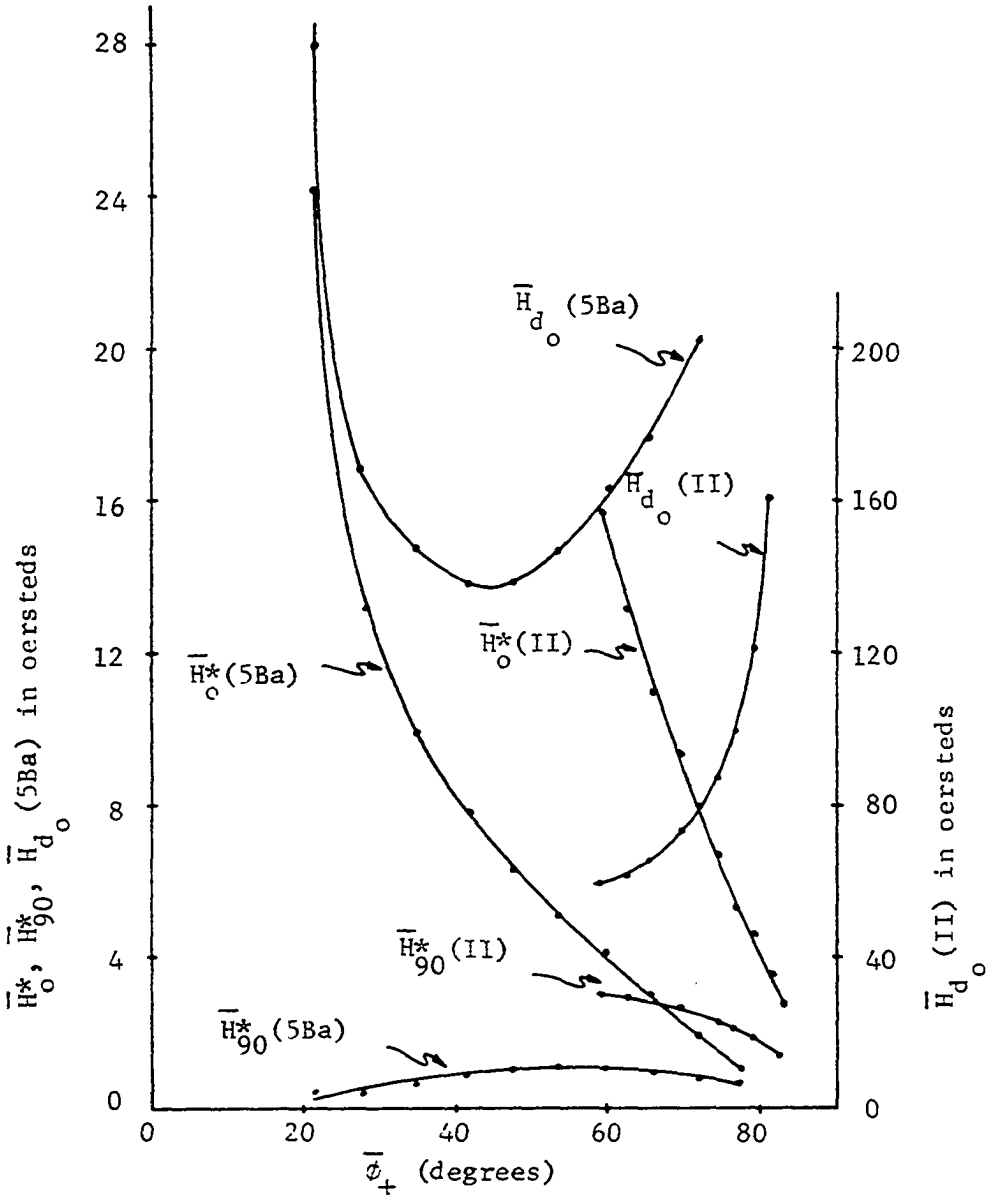

Figure 13. Internal fields versus $\bar{\phi}_+$ for EA and HA tickle fields for samples 5Ba and II

large enough ($\simeq$ 8mm in diameter) so that shape demagnetizing fields are negligible. This leaves only the $\overline{H}_{d_0}$ term which can be solved for and is plotted in Figure 13.

Note that the fields from sample II, for a given value of $\overline{\phi}_+$, are higher than those of sample 5Ba. This is to be expected because of the denser domain structure for the larger dispersed sample. The lower bound of these curves is dictated by the angle which describes their remanent ($H_{90} = 0$) configuration.

C. Ripple Behavior and Loss Characteristics as a Function of Bias Field

It is convenient in this discussion to consider the local magnetization variations for a zero field single domain configuration as being basically sinusoidal with an average wavelength of about 1-2 microns in a direction parallel to the mean $\vec{M}$. (A more exact description is given in the introduction.) This gives rise to the conventional picture of ripple (17, 23, 31) with the bands of magnetization alternating in direction by $\pm\overline{\varphi}$ (rms value of φ) about the mean direction of $\vec{M}$.

A description of the behavior of the ripple structure and a discussion of the loss phenomenon will be given as a dc field is increased from zero to saturation and back to zero along the average HA.

Consider the film initially in a single domain state and the bias field H_{90} increasing from zero. The ripple strips are initially parallel to the HA and rotate into the direction of H_{90}. It is noted that sample II exhibits a small amount of ripple pinning or locking at $H_{90} \simeq 0$. This is seen by the curve of Figure 5. Note the existence of loss at $H_{90} \geq 0$.

This comes about because of a lag of the ripple structure behind the HA tickle field. This in turn is due to the existence of small irreversible loss centers in this sample. These small potential wells inhibit the motion of the ripple structure. The result is that the local magnetization tends to lead the rotating ripple walls giving rise to induced stray fields which tend to inhibit the effect of the torque exerted by the tickle field. This means the measured values of $X'_{90,90}$, for $H_{90} \geq 0$, are actually less than they would be in the absence of ripple pinning.

The observation that the measured $X'_{90,90}$ curves (Figures 4 and 5) for both samples have a positive slope at $H_{90} \geq 0$, for a single domain configuration, is due to the existence of ripple. An explanation can be effected by considering two adjacent bands of the ripple structure. Assume that these bands, described by a bimodal angular distribution of $\pm\bar{\varphi}$ about a mean direction of $\bar{\phi}_+$, are noninteracting. This being the case it can be shown that the sum of the $X'_{90,90}$ contributions, from Equation 19, for the two bands and evaluated at $\bar{\phi}_+ \pm \bar{\varphi}$, is greater for $\bar{\phi}_+ \simeq 30^\circ$ than for $\bar{\phi}_+ = 0^\circ$. Evaluating $X'_{90,90}$ from Equation 19 by only substituting in values of $\bar{\phi}_+$, and not explicitly accounting for the ripple, results in a constant characteristic out to large values of $\bar{\phi}_+$.

The subsequent decrease in this function on the other side of the peak is primarily due to the presence of partial switching domains and the accompanying stray and induced locking fields. This is particularly true of sample II where, as discussed in the last section, it is believed labyrinth domains are prematurely propagating through the film at small angles to the EA at low values of H_{90}. This was substantiated by the

observation of $X''_{0,90}$ at these fields, as seen in Figure 10. Another reason for the decrease in $X'_{90,90}$ comes from the stray fields induced by the increasing ripple amplitude. These fields, from both the ripple structure and walls, provide effective net torques contrary to the action of the tickle field. Also, since the switched portions of the film are at larger angles to the ED, they provide a smaller moment arm to the tickle field, and therefore a decrease in ΔM_{90}.

Another observation demonstrating the greater dispersion (larger ripple wavelength and amplitude) of sample II as compared with 5Ba is the existence of HA loss, $X''_{90,90}$, for low values of H_{90}, including $H_{90} = 0$. This comes from irreversible ripple jumps under the influence of the tickle field (27, 28). Its noticeable occurrence in sample II is due to the more maze like ripple pattern which provides more potential loss centers or nodes than sample 5Ba. The existence of walls in this sample at an angle to the EA would also certainly contribute to this observed loss.

As H_{90} increases further the partially switched domain density grows (or is initiated as in sample 5Ba), as witnessed by the increase in EA loss, $X''_{0,90}$, Figures 10 and 11. This is eventually accompanied by an increase in $X''_{90,90}$ for both samples. The interpretation of this is that the wall density is increasing, with H_{90}, at a faster rate than these walls can rotate into parallel alignment with the EA.

A larger H_{90} causes the wall density to increase to the point that demagnetizing fields are induced by the tickle field which results in a dip or inflection in $X_{0,90}$ at about H_k. This process is followed by the

ripple and wall structure rotating into parallel alignment with the EA, which results in $X''_{90,90}$ going to zero. Above this in field space the small angle walls merge with the gross ripple structure whose wavelength and amplitude have increased to the point where it is difficult to tell ripple boundaries from walls (20). This structure has considerable stray field interactions taking place. However, at these fields it is believed that the ripple amplitude is a decreasing function of H_{90} while the wavelength remains relatively constant. This gives rise to a decrease in the stray fields and a relaxation of internal locking which results in a peak in the $X_{0,90}$ characteristics. A further increase in H_{90} causes a decrease in wavelength and amplitude such that the net restoring torques increase. This results in a decrease in $X_{0,90}$, as seen in Figures 10 and 11.

The decreasing characteristics are coincident with the increasing ones until just above H_k, as observed in Figures 10 and 11. The reason for the separation is due to a secondary ripple structure described by Hoffmann (22, 23), which initially comes into the picture at about $2H_k$. The primary structure remains, on the average, parallel to the EA. The secondary structure forms within the primary and is also composed of strips oriented perpendicular to the net magnetization within a strip. However, these strips are not parallel to the EA. The configuration resembles, in general, a very small angle splitting domain structure. As H_{90} approaches H_k, the primary wavelength and amplitude increase until the amplitude becomes large enough to induce considerable volume divergence throughout the film. According to Hoffmann (23, 41) this results in longitudinal stray fields, a ripple rearrangement (blocking), and then

ripple pinning or locking. The results of these actions are the peaks of the $X_{0,90}$ curves. Shortly below this vicinity of field space the primary ripple structure becomes the characteristic splitting domain structure, which occurs approximately at $H_{90} \simeq H_k$. This says the peak in the $X_{0,90}$ curves lies above H_k, as is seen in Figures 10 and 11.

The reason the decreasing curves do not experience a low field peak similar to the increasing characteristics is due to the fact the splitting domain walls are on the average always parallel to the EA, and much greater in density than the partial switching domains. This means no wall rotation takes place ($X''_{90,90}$ is essentially zero) and a considerably greater amount of wall pinning occurs. This is demonstrated in Figure 9 where a definite $\Delta\bar{\phi}_+$ difference between the two curves is observed.

The loss observed on the return characteristic of $X''_{90,90}$ of sample 5Ba at $H_{90} \geq 0$ is due to a Néel to Block wall transition (31) which occurs at these fields. The structure of sample II remains sufficiently locked up that this apparently is not observed.

D. Two Loss Mechanisms

The observation of two quite distinct peaks on the $X_{0,90}$ curves of sample 5Ba, seen in Figure 11, gives rise to the possibility of two distinct mechanisms responsible for the loss phenomenon. This is confirmed by loss measurements taken at various angles to the HA, which tends to accentuate the two processes. This in seen in Figure 14 for the low dispersion sample 5Ba. Both the increasing and decreasing characteristics were plotted. It is noted that as the angle of the field path rotates into the unstable region of field space (greater than 90^o) the two peaks

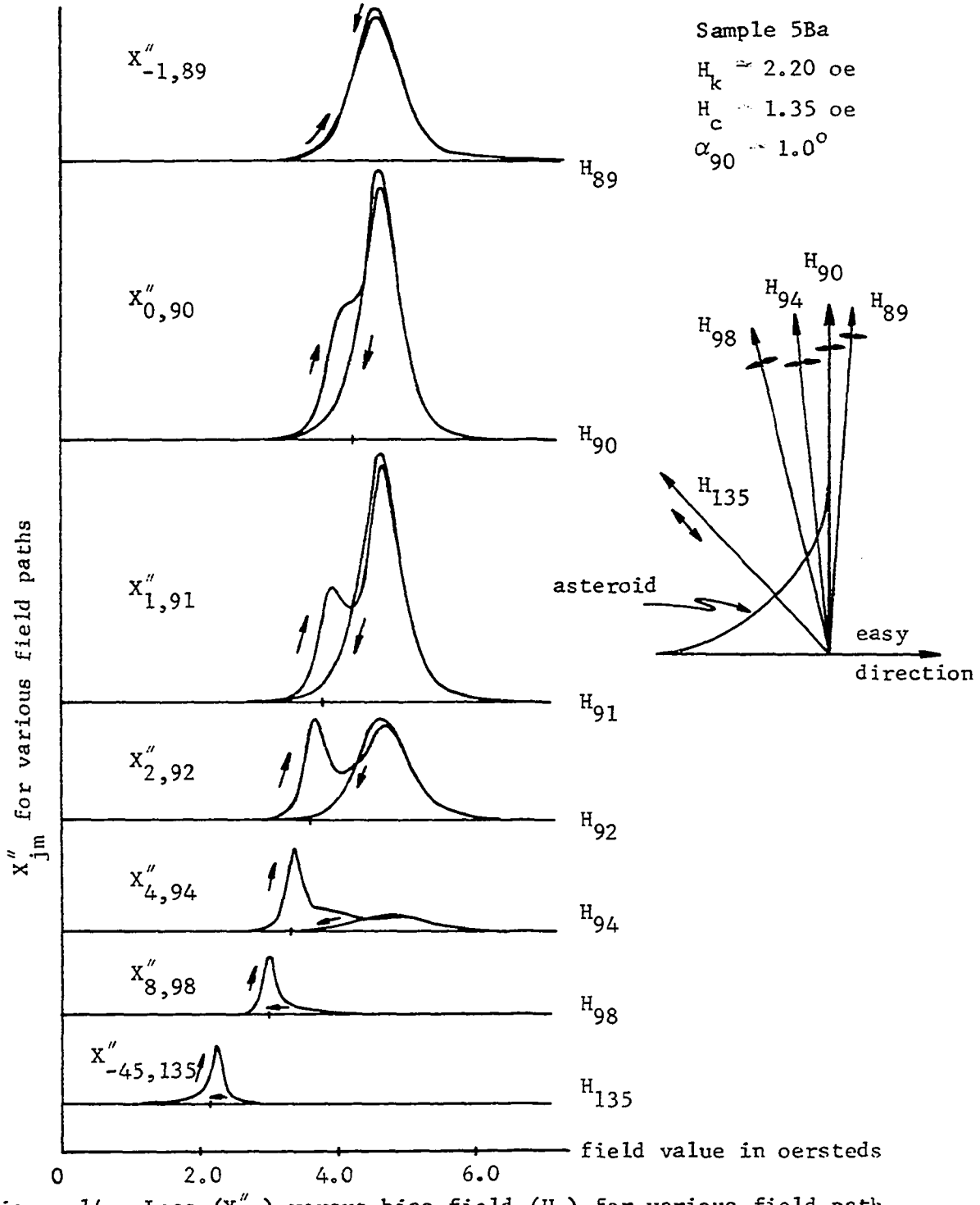

Figure 14. Loss (X''_{jm}) versus bias field (H_m) for various field path orientations. The field values of the intersections of the field paths with the asteroid are shown

become very distinct. As this angle increases the high field peak degenerates into a long tail and eventually nothing at all.

The first or low field peak represents loss due to the occurrence of labyrinth or partial rotation domains as the field point approaches or traverses the rotational switching threshold. This occurs at every crossing provided complete wall switching does not prematurely intervene. The magnetic structure of a sample similar to 5Ba was observed through the Bitter Pattern technique (31, 39). During this observation the field point was on an axis about 93^{o} from the ED and lying approximately on the asteroid boundary. The observations showed that relatively widely spaced walls were present. These walls disappeared for a subsequent increase in field magnitude. These observations substantiate the belief that the low field loss is due to wall motion. Note that the field values of the low peaks follow quite closely the field magnitudes of the asteroid for the respective angle. This includes the peak of the $X''_{-45,135}$ loss curve, which falls on the asteroid. As the angle of the field path rotates towards the ED, into stable field space, seen in Figure 14, the low field peak disappears. This indicates that the low peak is indeed due to the irreversible movement of domain walls, since partial switching drops off very rapidly as this field angle increases (from the HA) for low dispersion samples (42).

The high field peak comes about because of the very maze like ripple structure which exists at field values such as these. In this vicinity there are a maximum number of irreversible loss centers which are least constrained by stray field interactions. Note that the magnitude of this

loss is primarily a function of the orientation (azimuth) of the field path and very little a function of the field magnitude.

In regard to the variation of the peak magnitude of the loss curves as a function of angle of orientation of the field path it should be noted that the effective tickle field is also varying. This means that as the angle increases the component of the tickle field, which for these measurements is always applied perpendicular to the bias field, parallel to the walls and ripple striations is decreasing. This results in a decrease in the force on the walls and would explain part of the decrease in maximum value of loss. The one exception to this is $X''_{-45,135}$ where to achieve maximum loss the tickle field was applied parallel to the dc field.

A plot of the magnitude of the tickle field versus maximum loss at a fixed angle was plotted for both the low field and high field peaks. This is seen in Figure 15, where the hypothesis of two loss mechanisms is given considerable verification. These measurements were done on sample 101, another low dispersion sample.

E. Effect of Shape on Two Rectangular Samples

This section deals very briefly with two films of rectangular shape. The dimensions are approximately 1mm x 13mm so the shape component of the net restoring torque and subsequent field can not be neglected in Equations 14 and 17. This comes about because the small dimension is small enough so that demagnetizing type fields from magnetization discontinuities at the edges are appreciable. These films were cut from the same large film, and from the same approximate location in that film,

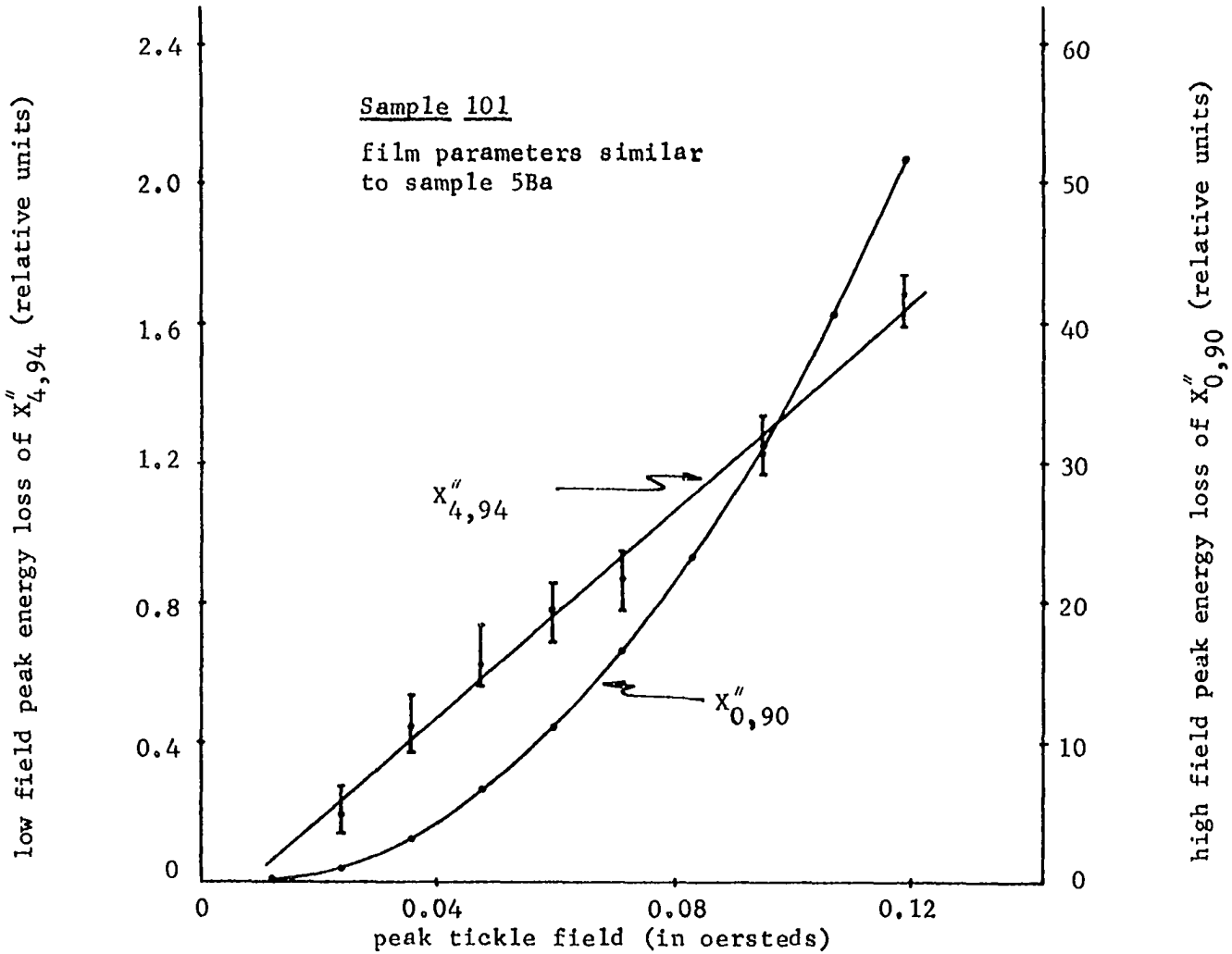

Figure 15. Peak loss versus peak tickle field for 90° (high field peak) and 94° (low field peak) field path orientations

as sample 5Ba.

Plots of $\bar{X}_{90,90}$ are shown in Figures 16 and 17, and plots of $\bar{X}_{0,90}$ are in Figures 18 and 19 for samples 5Bb and 5Bc respectively. These pictures show the effect of the demagnetizing fields in that the curves of 5Bb appear to be effectively expanded to higher field values from those of sample 5Bc. H_k for the round sample 5Ba was used as the common H_{90} normalization constant. A very graphic illustration of the effect of these fields is shown in Figure 20. This is a plot of $\bar{M}_{90}/M$ vs normalized H_{90}. Also included is the same plot for the round sample 5Ba, for comparison. Note the curves from the rectangular samples are on both sides of 5Ba.

An explanation of these observations can be presented by considering the angle $\bar{\phi}_+$ to have the same interpretation as in Section C, i.e. the angle between the mean direction of $\vec{M}$ and the ED. For the increasing curves of sample 5Bc, the demagnetizing field is proportional to $\cos\bar{\phi}_+$ and the static torque to $\sin 2\bar{\phi}_+$. It is in the same direction as H_{90} ($\cos\bar{\phi}_+$ static torque dependence) and therefore tends to aid this field, or more appropriately, decrease the effect of the uniaxial anisotropy restoring torque. The result is an effective shift of these curves (Figures 17 and 19) to lower field values as compared to those of the round sample 5Ba (Figures 4, 11 and 20). The decreasing characteristics for this sample experiences a demagnetizing field again proportional to $\cos\bar{\phi}_+$, where $\bar{\phi}_+$ is now the direction of $\vec{M}$ in a strip domain. This field tends to reinforce the torque due to wall fields and causes a high remanent $\bar{M}_{90}$ (Figures 17 and 20).

Sample 5Bb is the reverse of 5Bc in that the increasing curve gives

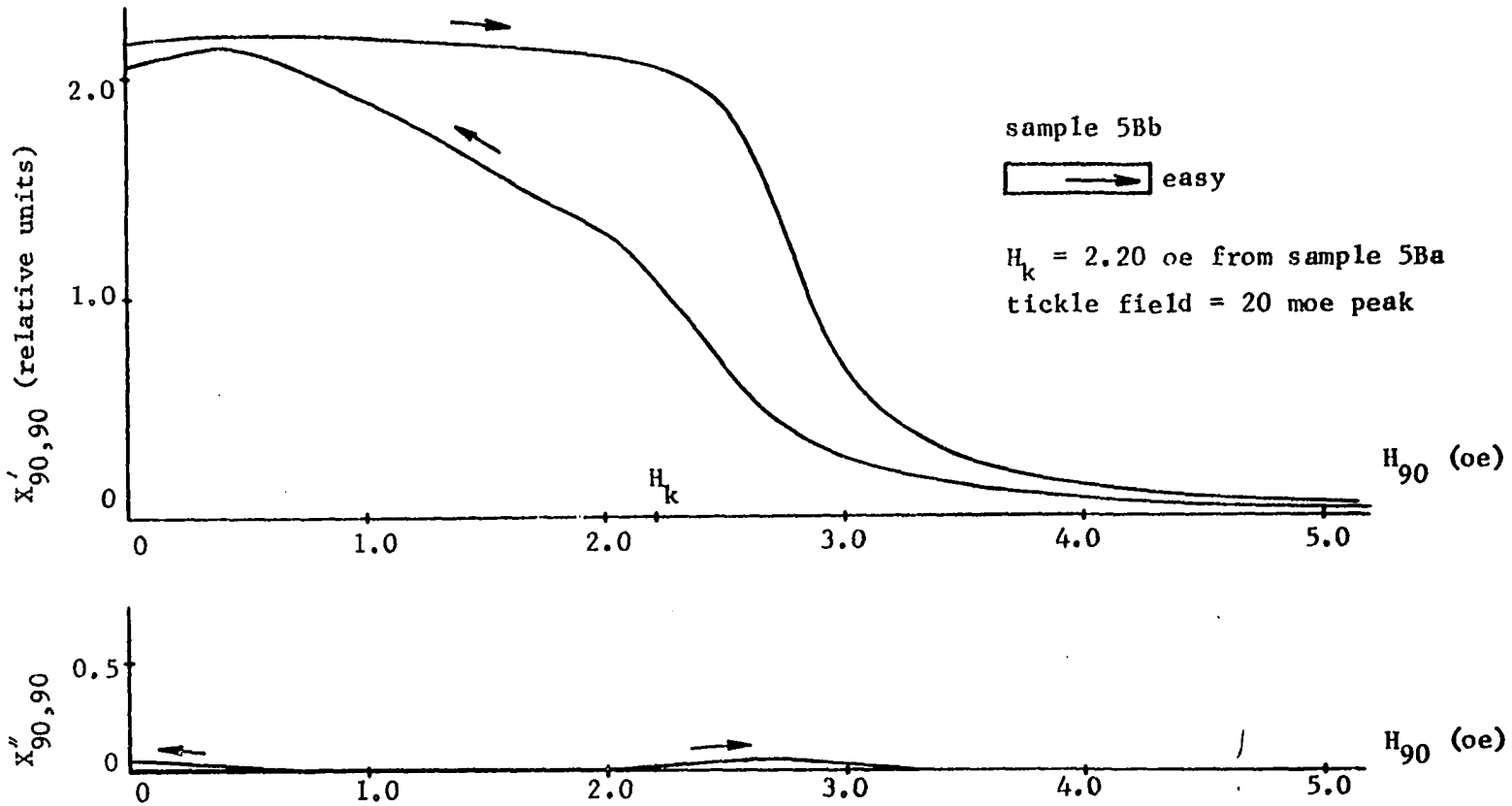

Figure 16. Real ($X'_{90,90}$) and imaginary ($X''_{90,90}$) parts of $X_{90,90}$ versus H_{90}

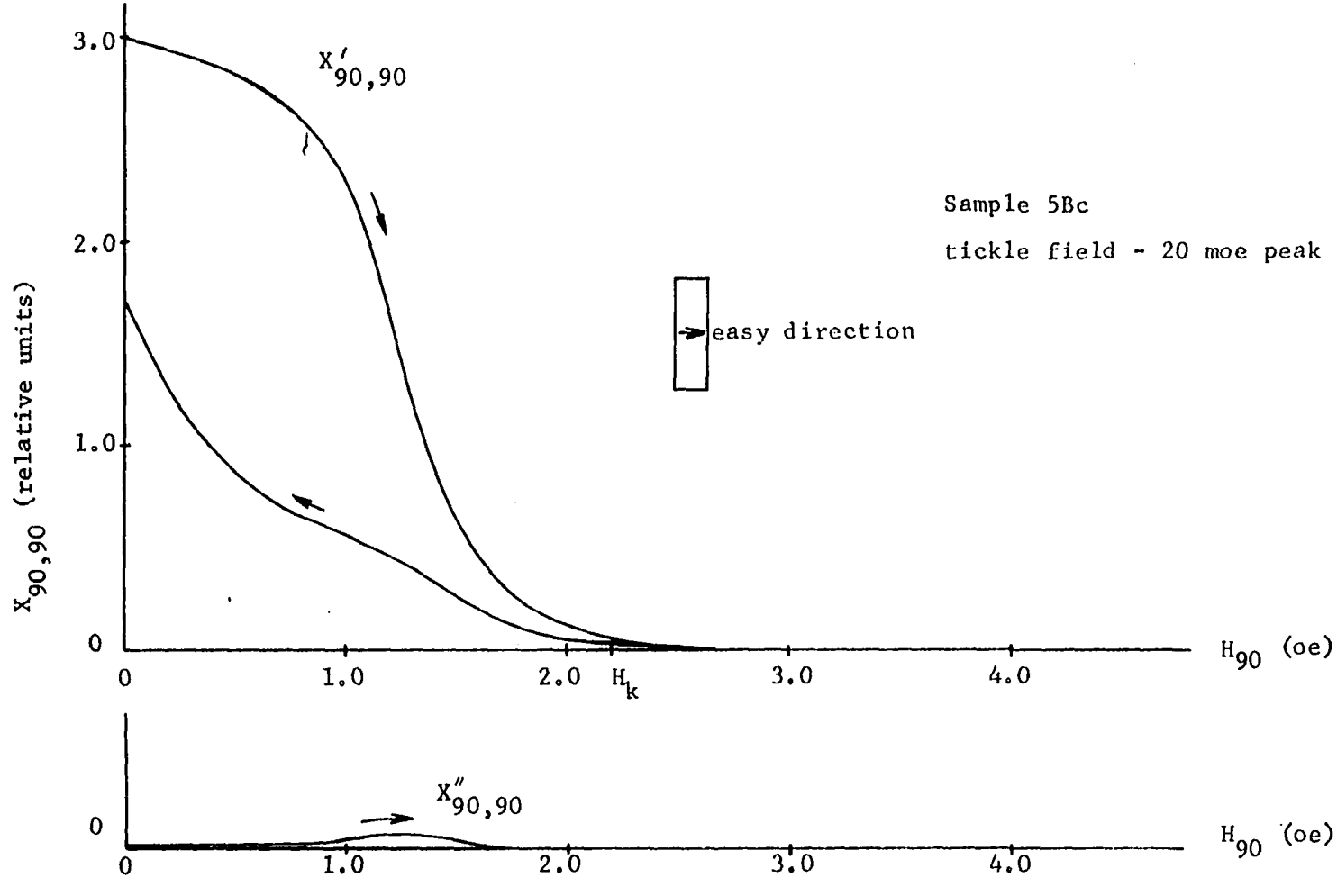

Figure 17. Real ($X'_{90,90}$) and imaginary ($X''_{90,90}$) parts of $X_{90,90}$ versus H_{90}. The value of H_k is that of the round sample 5Ba

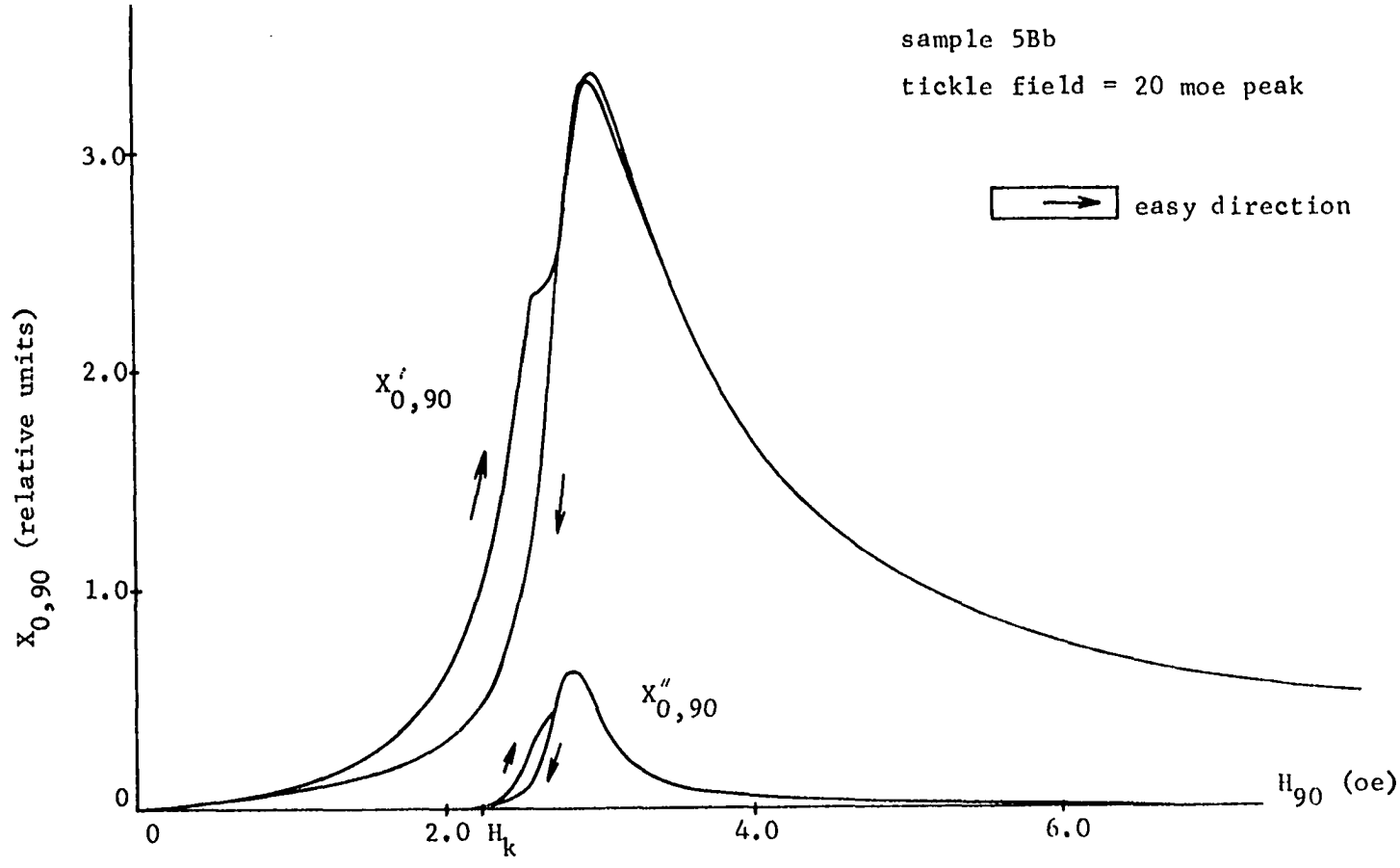

Figure 18. Real ($X'_{0,90}$) and imaginary ($X''_{0,90}$) parts of $X_{0,90}$ versus H_{90}. The value of H_k is that of the round sample 5Ba

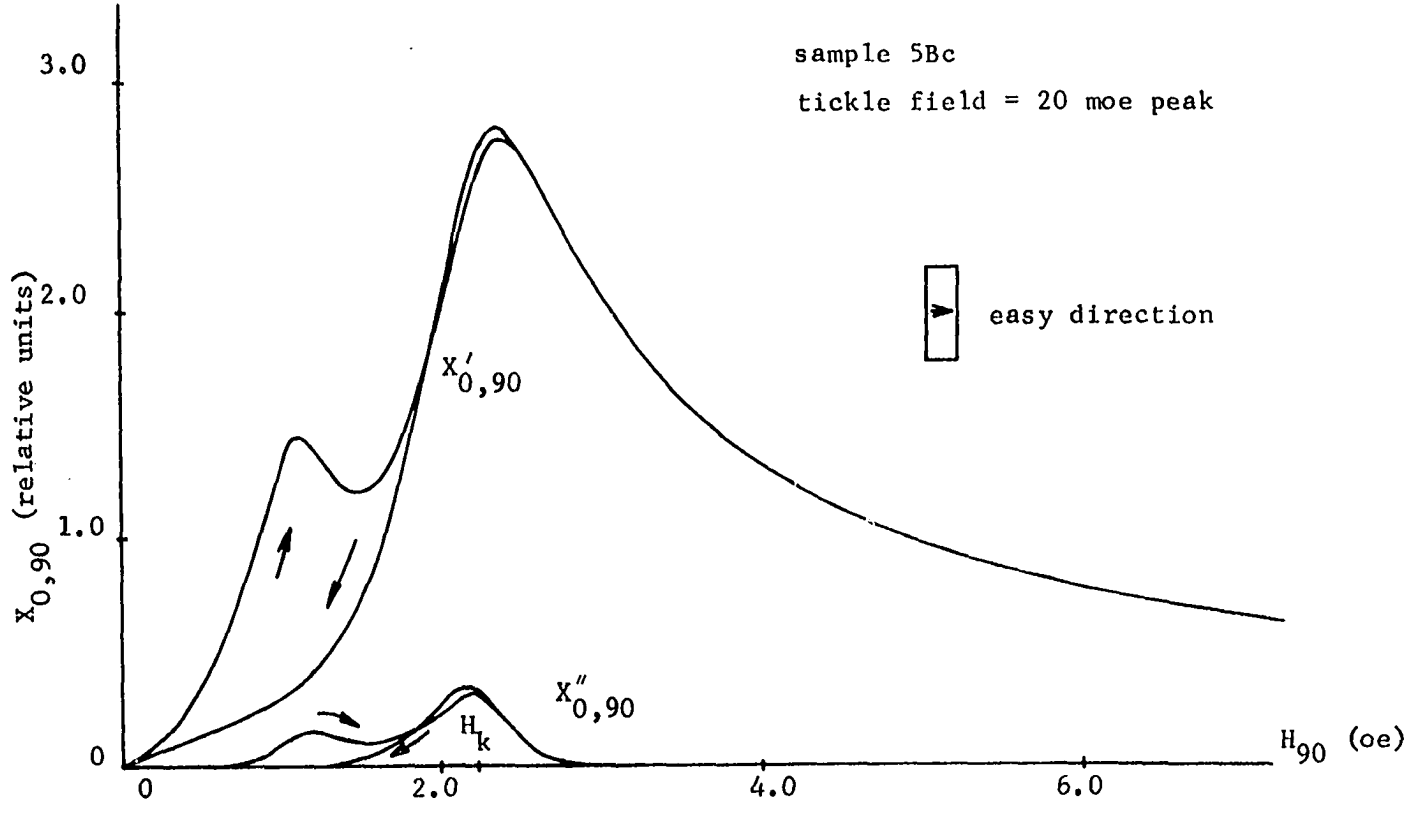

Figure 19. Real ($X'_{0,90}$) and imaginary ($X''_{0,90}$) parts of $X_{0,90}$ versus H_{90}. The ordinate scale on $X''_{0,90}$ is 2.08 times that of $X'_{0,90}$. The value of H_k is that of the round sample 5Ba

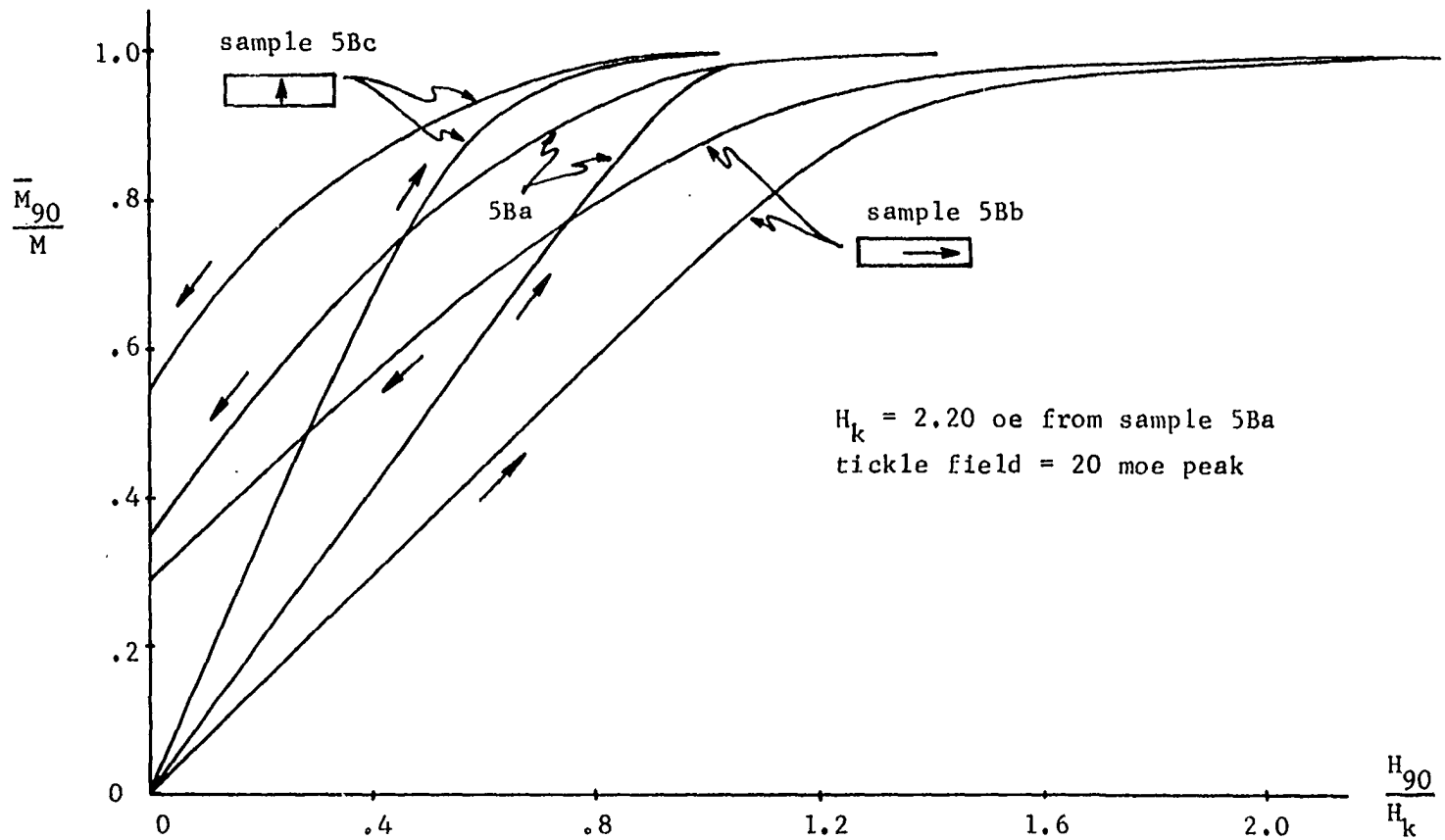

Figure 20. Measured values of $\bar{M}_{90}/M$ versus H_{90}/H_k for samples 5Ba, 5Bb, and 5Bc. The value of H_k used in field normalization was that of sample 5Ba

rise to a demagnetizing field proportional to $\sin\bar{\phi}_+$ which in turn results in a positive static torque ($\sin 2\bar{\phi}_+$) which tends to reinforce the effect of the uniaxial anisotropy, or decrease the effect of H_{90}. This results in a shift towards higher field values, as seen in Figures 16, 18 and 20.

Another point of comparison concerns the values of $\bar{X}'_{90,90}$ at $H_{90} = 0$ for the two samples (the vertical scales are the same on the two curves), in Figures 16 and 17. The value for sample 5Bc is higher than that of 5Bb due to the inhibiting effect of the induced demagnetizing fields on the torque from the applied ΔH_{90}. This results in a smaller corresponding $\overline{\Delta M}_{90}$. However, for 5Bc, the torque due to the tickle field is effectively aided by the induced fields, which results in a larger $\overline{\Delta M}_{90}$.

Note the rapid drop off of $X'_{90,90}$ for sample 5Bc. This is due to partial switching from the propagation of edge domains. The induced field aids considerably in their formation and propagation. Just the opposite is true of 5Bb, as witnessed by the relatively flat curve, Figure 16.

F. Comparison of Experiment and Theory

This section will involve a comparison between part of the experimental approach of this thesis and some of the theoretical results of Hoffmann (23).

The first relationship to be compared is X_{jj} vs H_j. Hoffmann (23) presented a mathematical expression for X_{jj} using his linear theory, which stipulated that the ripple amplitude, φ_j, be kept small. This theory involved discarding a term proportional to longitudinal stray fields on the grounds that it would be small for small values of ripple amplitude, i.e. less then approximately 2^o (41). If H_{90} is kept greater than about $1.5H_k$ and H_0 greater than about $.5H_k$, the approximation should not be

violated along those field axes.

Hoffmann's expression for this relationship is

$$X_{jj} = (\text{const})(H_j \pm H_k)^{-1.75}$$

where if j = 0, the + sign is used and if j = 90, the - sign is used. The curve of X_{90} versus $H_{90} - H_k$, plotted from the experimental data of this investigation for a film similar to sample 5Ba (from the same large film) on log-log paper, gave a slope of -1.76, and is seen in Figure 21a. This shows the very good agreement between experiment and theory.

Another version of the same curve is seen in Figure 21b, and is $(X'_{90,90})^{-1.75}$ vs H_{90}. This curve is interesting in that the break-away in the behavior of the ripple structure from the linear theory is observed. This shows the effects of the large ripple amplitude and resulting stray fields. The difference in field values between the linear extrapolated curve and the actual experimental curve show these increasing stray field effects.

Another functional relationship which was compared was $\bar{\varphi}_{90}$ as a function of $H_{90} - H_k$, where $\bar{\varphi}_{90}$ is the rms value of the ripple angle. This was plotted in Figure 7, Section B. The relationship from Hoffmann (23) was

$$\bar{\varphi}_{90} = (\text{const})(H_{90} - H_k)^{-3/8} \qquad (5)$$

The constant was evaluated from the experimental point $\bar{\varphi}_{90} = 2.83^\circ$ and $H_{90} - H_k = 1.61$. This point was chosen because smaller angles involved more error from the integration process, and larger angles approached nonlinear effects not included in the theory. The agreement was fairly good.

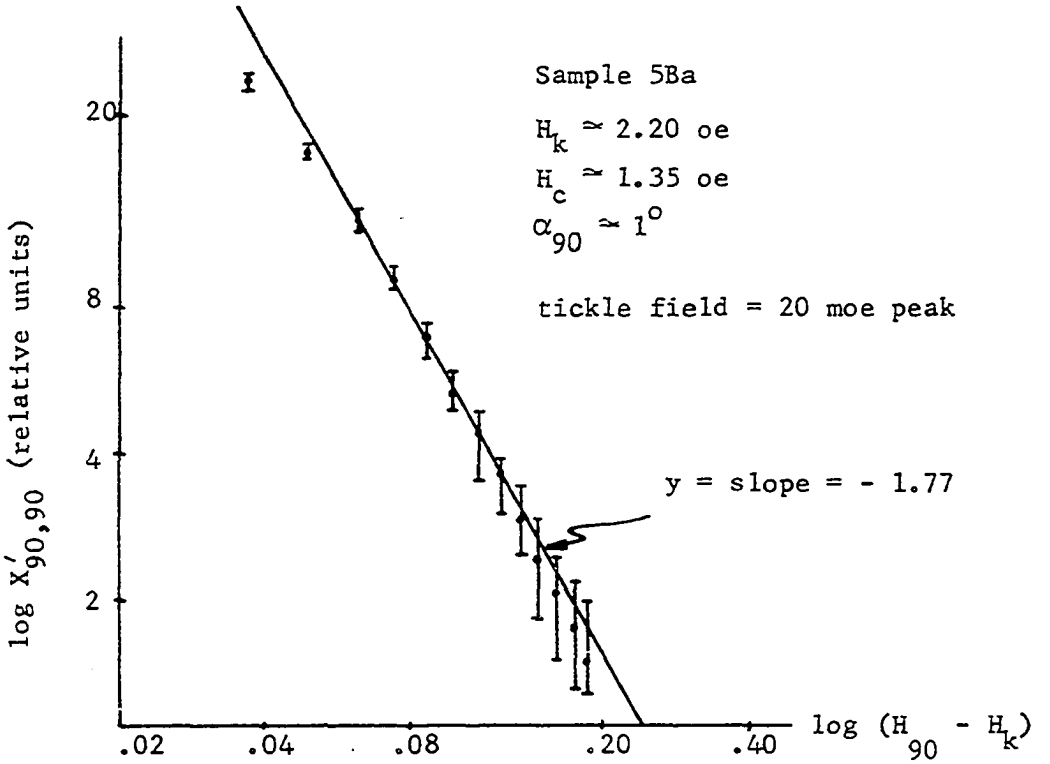

Figure 21a. Determination of exponent y in $X'_{90,90} = (\text{const})(H_{90} - H_k)^y$

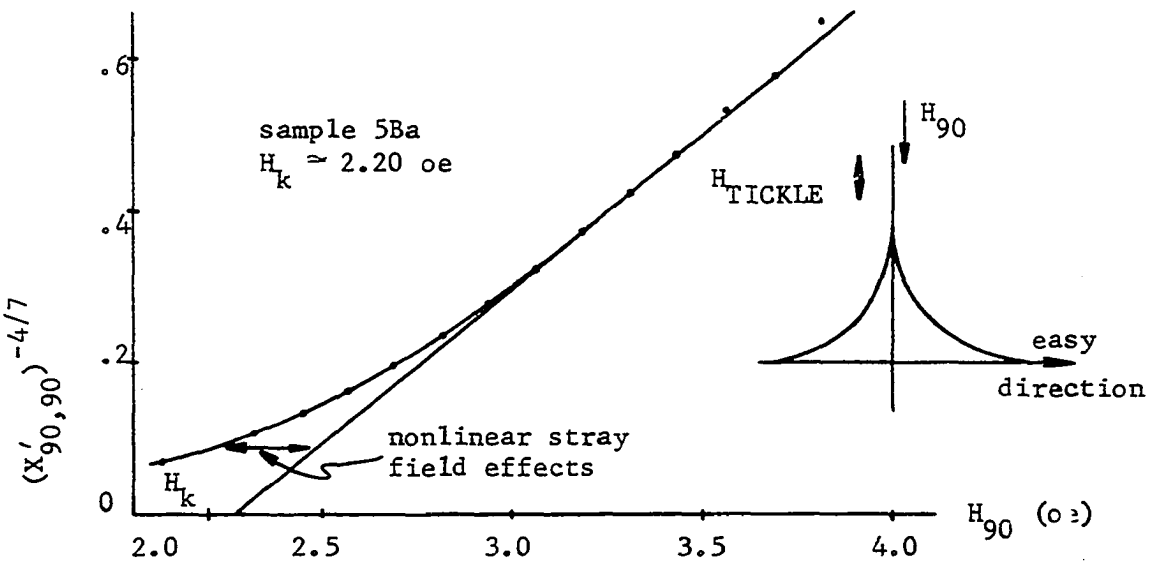

Figure 21b. $(X'_{90,90})^{-4/7}$ versus 90° bias field

The last variable compared was the blocking field (23, 41) which was believed to occur at about the peak of the $X'_{0,90}$ curve, or $H_{90} \simeq 1.14H_k$ for sample 5Ba. However, due to uncertainties in many of the constants the comparison was poor ($\simeq 3H_k$). The technique used was first of all an evaluation of the structure constant, S, from Hoffmann's expression for $\bar{\varphi}_{90}$ as a function of H_{90} (23). From this a value for the blocking field can be found from an expression in References 23 and 41. Both expressions require knowing the uniaxial anisotropy and exchange constants, the film thickness, saturation magnetization and H_k. Knowledge of these constants and an accurate point on the $\bar{\varphi}$ - H curve from which S might be determined are needed for a good evaluation of the field.

IV. CONCLUSIONS

This investigation showed that from measurements of the real part of the complex bias susceptibility, χ'_{jj}, under the influence of j-axis tickle and bias fields, where j = 0° and 90°, it was possible to obtain values of the average rms ripple angle $\bar{\varphi}_j$ for a region of field space. This was accomplished by integration of the experimentally determined $\bar{X}_{jj}$ - H_j curves. The pertinent region of field space is defined by fields which are sufficiently high that $\bar{\varphi}_j$ is kept small enough so induced stray fields are negligible. Correlation between these experimental results and a theoretical prediction of Hoffmann (23) was good.

A technique was devised to obtain a quantitative measure of some of the internal magnetostatic fields in a magnetic film. The process was initiated by an integration procedure similar to that mentioned above, but in this case only the $\bar{X}'_{90,90}$ - H_{90} curve was used. This gave rise to a measure of the average angular orientation of the magnetization, $\bar{\phi}_+$, for any 90° field point within a strictly increasing sweep of H_{90} from zero (single domain state) to saturation and a decreasing sweep from saturation back to zero.

For values of $H_{90} < H_k$, on the decreasing characteristic, $\bar{\phi}_+$ was interpreted as the average angular orientation of $\vec{M}$ within the strip domains. $\bar{\phi}_+$ also gave a measure of the average orientation of $\vec{M}$, for low dispersion films, when the film was initially set in a single domain state.

Mathematical expressions for $X'_{90,90}$ and $X'_{0,90}$ were found which included the various internal fields. These fields were solved for, although complete separation was not rigorously possible. It was seen that

internal demagnetizing fields, induced by the application of a tickle field parallel to the EA, were largely responsible for the observation that $X_{0,90}$ in the strip domain state was less than it was in a single domain state for the same angle $\bar{\phi}_+$. These fields also are largely responsible for the $X_{0,90}$ peaks being shifted to an H_{90} value higher than H_k.

Measurements of the imaginary or loss part of the bias susceptibility, X''_{jm} showed that the loss phenomenon takes place by two separate mechanisms, which are very field sensitive. It is believed that the low field loss occurs through movements of partial-switching-domain walls. The high field loss is attributed to irreversible rearrangements of the very dispersed ripple structure. These two processes are seen in Figure 13, where the magnitude of the two loss peaks are plotted as a function of the magnitude of the tickle field.

A comparison between the theoretical work of Hoffmann and the present experimental approach showed good agreement in the functional relationship between $X_{90,90}$ and H_{90}. This relationship was that $X_{90,90}$ was proportional to $(H_{90} - H_k)^{-7/4}$.

Two films of rectangular shape were also examined and the effect of shape anisotropy was observed. The resulting curves were compared with those of a round sample which was cut from the same vicinity in the large parent film as the two rectangular ones.

V. BIBLIOGRAPHY

1. Stoner, E. C. and E. P. Wohlfarth. A mechanism of magnetic hysteresis in heterogeneous alloys. Phil. Trans. Roy. Soc. London 240A: 599-642. 1948.

2. Crowther, T. S. Techniques for measuring the angular dispersion of the easy axis of magnetic films. M.I.T. Lincoln Laboratory Group Report 51-2. February 1959.

3. Smith, D. O. Static and dynamic behavior of thin permalloy films. J. Appl. Phys. 29: 264-273. 1958.

4. Olson, C. D. and A. V. Pohm. Flux reversal in thin films of 82% Ni, 18% Fe. J. Appl. Phys. 29: 274-282. 1958.

5. Torok, E. J., R. A. White, A. J. Hunt and H. N. Oredson. Measurement of the easy-axis and H_K probability density functions for thin ferromagnetic films using the longitudinal permeability hysteresis loop. J. Appl. Phys. 33: 3037-3041. 1962.

6. Crowther, T. S. Angular and magnitude dispersion of the anisotropy in magnetic films. J. Appl. Phys. 34: 580-587. 1963.

7. Torok, E. J. Origin and effects of local regions of complex biaxial anisotropy in thin ferromagnetic films with uniaxial anisotropy. J. Appl. Phys. 36: 952-960. 1965.

8. Harte, K. J. Theory of magnetization ripple in ferromagnetic films. J. Appl. Phys. 39: 1503-1524. 1968.

9. Ehresman, V. A. and C. D. Olson. Variations in anisotropy magnitude and magnetization direction in planar films under equilibrium conditions. J. Appl. Phys. 37: 1287-1289.

10. Smith, D. O. Negative anisotropy in nickel-iron films. Appl. Phys. Letters 2: 191-193. 1963.

11. Doyle, W. D., J. E. Rudisill and S. Shtrikman. Unidirectional hysteresis in thin permalloy films. J. Appl. Phys. 33: 1162-1163. 1962.

12. Torok, E. J., H. N. Oredson and A. L. Olson. Local regions with biaxial anisotropy in thin polycrystalline ferromagnetic films with uniaxial anisotropy. J. Appl. Phys. 35: 3469-3481. 1964.

13. Coren, R. L. and H. J. Juretschke. Tech. Report No. 9, Physics Department, Polytechnic Institute of Brooklyn. 1960. Original not available, cited in Cundall, J. A. and A. P. King. Comparison of magnetic measurements and theoretical predictions for nickel-iron films over a wide composition range. Phys. Stat. Sol. 16: 613-619. 1966.

14. Cundall, J. A. and A. P. King. Comparison of magnetic measurements and theoretical predictions for nickel-iron films over a wide composition range. Phys. Stat. Sol. 16: 613-619. 1966.

15. Uchiyama, S., T. Fujii, M. Masuda and Y. Sakaki. Origin of the periodic component of anisotropy dispersion in Ni-Fe films II. Japan J. Appl. Phys. 6: 512-515. 1967.

16. Hale, M. E., H. W. Fuller and H. Rubinstein. Magnetic domain observations by electron microscopy. J. Appl. Phys. 30: 789-791. 1959.

17. Fuller, H. W. and M. E. Hale. Determination of magnetization distribution in thin films using electron microscopy. J. Appl. Phys. 31: 238-248. 1960.

18. Boersch, H. and H. Raith. Electronenmikroskopische abbildung weisscher bezirke in dünnen ferromagnetischen schichten. Naturwissenschaften 46: 574-575. 1959.

19. Cohen, M. S. Influence of anisotropy dispersion on magnetic properties of Ni-Fe films. J. Appl. Phys. 34: 1841-1847. 1963.

20. Cohen, M. S. Magnetic measurements with Lorentz microscopy. I.E.E.E. Trans. Magnetics MAG-1: 156-167. 1965.

21. Rother, H. Berechnung des magnetisierungs-'Ripple' in ferromagnetischen dunnen schichten. Z. Physik 179: 229-243. 1964.

22. Hoffmann, H. Quantitative calculation of the magnetic ripple of uniaxial thin permalloy films. J. Appl. Phys. 35: 1790-1798. 1964.

23. Hoffmann, H. Theory of magnetization ripple. I.E.E.E. Trans. Magnetics MAG-4: 32-38. 1968.

24. Joenk, R. J. Magnetization ripple in ferromagnetic films. A survey of recent theoretical work. IBM Research Report RC-1281. August 1964.

25. Harte, K. J. Spin wave effects in the magnetization reversal of a thin ferromagnetic film. Lincoln Laboratory Technical Report 364. August 1964.

26. Callen, H. B., R. L. Coren and W. D. Doyle. Magnetization ripple and arctic foxes. J. Appl. Phys. 36: 1064-1066. 1965.

27. Feldtkeller, E. Ripple hysteresis in thin magnetic films. J. Appl. Phys. 34: 2646-2652. 1963.

28. Feldtkeller, E. Small-amplitude ripple hysteresis in magnetic thin films. Int. Conf. on Magnetism Proc., Nottingham, England, 1964: 837-842. 1964.

29. Spain, R. J. and I. B. Puchalska. Mechanism of ripple formation in thin films. J. Appl. Phys. 35: 824-825. 1964.

30. Baltz, A. The effect of alloy composition on the magnetization ripple of permalloy films. Int. Conf. on Magnetism Proc., Nottingham, England, 1964: 845-846. 1964.

31. Middelhoek, S. Ferromagnetic domains in thin Ni-Fe films. Amsterdam, Holland, Drukkerij Wed. G. Van Soest N.V. 1961.

32. Oredson, H. N. and E. J. Torok. Causes of the inhomogeneity in the magnitude of the anisotropy field in thin nickel-iron films. J. Appl. Phys. 36: 950-951. 1965.

33. Leaver, K. D., M. Prutton and F. G. West. Susceptibility measurements and the magnetocrystalline anisotropy of polycrystalline ferromagnetic films. Phys. Stat. Sol. 15: 267-276. 1966.

34. Baltz, A. and W. D. Doyle. Effect of crystallite size and orientation on the magnetization ripple in permalloy films. J. Appl. Phys. 35: 1814-1818. 1964.

35. Harte, K. J., M. S. Cohen, G. P. Weiss and D. O. Smith. Origin of quadrature flux in magnetic films. Phys. Stat. Sol. 15: 225-231. 1966.

36. Prutton, M. The transverse susceptibility of single-crystal ferromagnetic films. J. Appl. Phys. 39: 1153-1154. 1968.

37. Leaver, K. D. Susceptibility and magnetization ripple in polycrystalline magnetic films. J. Appl. Phys. 39: 1157-1158. 1968.

38. Scott, W. T. The physics of electricity and magnetism. New York, N.Y., John Wiley and Sons, Inc. 1959.

39. Chikazumi, S. Physics of magnetism. New York, N.Y., John Wiley and Sons, Inc. 1964.

40. Slichter, C. P. Principles of magnetic resonance. New York, N.Y., Harper and Row. 1963.

41. Hoffmann, H. Stray fields in thin magnetic films. I.E.E. Trans. Magnetics MAG-2: 566-570. 1966.

42. Middelhoek, S. Static reversal processes in thin Ni-Fe films. IBM Journal of Research and Development 6: 394-406. 1962.

VI. ACKNOWLEDGMENTS

The author wishes to express his sincere thanks to Dr. Arthur V. Pohm for his invaluable guidance and encouragement. He would also like to thank Dr. Arthur C. Sharp and Dr. Robert L. Samuels for their help in designing and constructing the equipment and in taking much of the data. Thanks also goes to Mr. William D. Thomas for drafting the figures and Mrs. Axel Wibholm for her help in the final preparation of this thesis.